Supplement of Atmos. Chem. Phys., 25, 14449–14478, 2025 https://doi.org/10.5194/acp-25-14449-2025-supplement © Author(s) 2025. CC BY 4.0 License.





Supplement of

Towards an improved understanding of the impact of clouds and precipitation on the representation of aerosols over the Boreal Forest in GCMs

Sini Talvinen et al.

Correspondence to: Sini Talvinen (sini.talvinen@uef.fi) and Daniel G. Partridge (d.g.partridge@exeter.ac.uk)

The copyright of individual parts of the supplement might differ from the article licence.

Table of contents

S1 Summary of aerosol parametrizations in UKESM1 and ECHAM-SALSA	2
S1.1 Modal scheme in UKESM1	2
S1.2 Sectional scheme in ECHAM-SALSA (SALSA-module)	3
S2 Summary of wet scavenging parametrizations in UKESM1 and ECHAM-SALSA	5
S2.1 Below cloud scavenging (below-cloud impaction scavenging)	5
S2.2 In-cloud impaction scavenging	5
S2.3 Nucleation scavenging/aerosol activation	5
S2.4 Convective plume scavenging in UKESM1	6
S3 Utilised variables from the GCMs, data availability and average concentrations	7
S4 Representability of UKESM1 and ECHAM-SALSA amongst larger group of GCMs	10
S4.1 ECHAM-HAM	11
S4.2 ECHAM-HAM-P3	12
S4.3 CAM5	12
S.4.4 NorESM	12
S5 Additional figures and tables supporting the main results	14
S6 How well RH describes the in-cloud conditions in the GCMs?	26
References	28

S1 Summary of aerosol parametrizations in UKESM1 and ECHAM-SALSA

S1.1 Modal scheme in UKESM1

by illustration of the aerosol modes in Figure S1.

The aerosol scheme in UCKA can be run in multiple configurations. In this work, Global Model of Aerosol Processes (GLOMAP; Mann et al., 2010; Mulcahy et al., 2020) is used within UCKA, consisting total of five modes (Table S1, Figure S1) in which Aitken mode has both insoluble and soluble components, rest of the modes being soluble (Abraham et al., 2018). In addition, within UKESM1, the organic carbon (OC) from the UKCA aerosol scheme is converted to total organic matter (OM) by multiplying with factor of 1.4. Sulfate (SO4) in UKESM1 is represented by sulfuric acid (H2SO4), which we have converted to SO4 by multiplying it with the ratio of the mass mixing ratios of SO₄ and H₂SO₄ by $\frac{M_{SO_4}}{M_{H_2SO_4}} = \frac{96.06 \frac{g}{mol}}{98.079 \frac{g}{mol}} = 0.9794146$. Dust in UKESM1 is simulated separately from the other aerosols using the CLASSIC dust scheme (Bellouin et al., 2011). This scheme is based on the descriptions from Woodward (2001). Summary of the UKESM1 aerosol scheme is presented in Table S1, the abbreviations are explained in Table S2 followed

Table S1 Summary of the modes in the aerosol scheme used in UKESM1. GSD refers to geometric standard deviation. Abbreviations for the composition are explained in the Table S2 Note that dust aerosols are simulated separately following Woodward (2001) thus not included in this table.

Mode name and	Diameter	Composition	GSD for particle size
solubility	range (nm)		distribution
Nucleation soluble	< 10	SO4, OC/OM	1.59
Aitken soluble	10-100	SO4, BC, OC/OM	1.59
Aitken insoluble	10-100	BC, OC/OM	1.59
Accumulation soluble	100-500	SO4, SS, BC, OC/OM	1.4
Coarse soluble	500-10000	SO4, SS, BC, OC/OM	2.0

Table S2 Explanation of the abbreviations used in Tables S1 and S3

Species	Explanation
SO4/SU	sulfate
OC/OM	organic carbon/organic matter
BC	black carbon
SS	sea salt
DU	dust

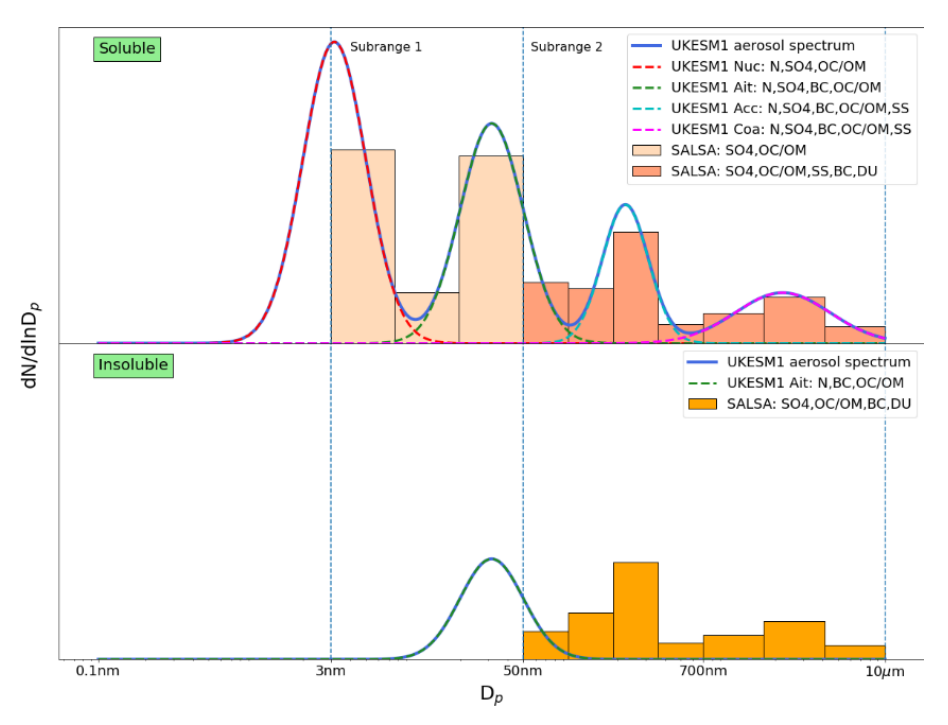


Figure S1 Schematic illustrating the aerosol schemes in UKESM1 (modal) and ECHAM-SALSA (noted as SALSA, sectional). Note that dust in UKESM1 is simulated separately following Woodward (2001), thus not being illustrated in this schematic. The abbreviations are presented in Table S2.

S1.2 Sectional scheme in ECHAM-SALSA (SALSA-module)

Aerosol microphysics for SALSA2.0 are presented in Kokkola et al. (2018). The size classes are visualised in Figure S1 and details of the composition and size ranges are given in Table S3. As in UKESM1, the organic carbon (OC) from the aerosol scheme is converted to total organic matter (OM) by multiplying with factor of 1.4.

Table S3 Summary of the SALSA2.0 microphysics scheme. For each range, geometric mean diameter (GMD) is also given. Abbreviations for the composition are given in Table S2 in the section above. Note that both insoluble and soluble modes in ECHAM-SALSA can activate as cloud droplets as their solubility is either "less soluble" (noted here as insoluble for conciseness) or "more soluble" (noted here as soluble).

Bin name and solubility	Diameter range	Composition	GMD for the range (nm)
	(nm)		
1a1, soluble	3.0-7.7	SO4, OC/OM	4.81
1a2, soluble	7.7-19.6	SO4, OC/OM	12.28
1a3, soluble	19.6-50.0	SO4, OC/OM	31.30
2a1, soluble	50.0-97.6	SO4, OC/OM, SS, BC, DU	69.86
2a2, soluble	97.6-187.0	SO4, OC/OM, SS, BC, DU	135.10
2a3, soluble	187.0-362.0	SO4, OC/OM, SS, BC, DU	261.97
2a4, soluble	362.0-700.0	SO4, OC/OM, SS, BC, DU	503.39
2a5, soluble	700-1700	SO4, OC/OM, SS, BC, DU	1090.87
2a6, soluble	1700-4120	SO4, OC/OM, SS, BC, DU	2646.51
2a7, soluble	4120-10000	SO4, OC/OM, SS, BC, DU	6418.72
2b1, insoluble	50.0-97.6	SO4, OC/OM, BC, DU	69.86

2b2, insoluble	97.6-187.0	SO4, OC/OM, BC, DU	135.10
2b3, insoluble	187.0-362.0	SO4, OC/OM, BC, DU	261.97
2b4, insoluble	362.0-700.0	SO4, OC/OM, BC, DU	503.39
2b5, insoluble	700-1700	SO4, OC/OM, BC, DU	1090.87
2b6, insoluble	1700-4120	SO4, OC/OM, BC, DU	2646.51
2b7, insoluble	4120-10000	SO4, OC/OM, BC, DU	6418.72

S2 Summary of wet scavenging parametrizations in UKESM1 and ECHAM-SALSA

S2.1 Below cloud scavenging (below-cloud impaction scavenging)

The parameterisation of below cloud wet scavenging by rain in both GCMs follows the approach originally presented by Slinn (1983), where a look-up table for collection efficiencies based on geometric mean dry radius of the aerosol mode is used. Raindrop sizes in both UKESM1 and ECHAM-SALSA are distributed using the Marshal-Palmer distribution (Marshal and Palmer, 1948).

For below cloud wet scavenging by snow, ECHAM-SALSA uses the approach from Slinn (1983) whereas the UKESM1 implementation follows Wang et al. (2011), where the fraction removed is a power law with coefficients prescribed for each mode defined as:

$$k = aP^b, (S1)$$

where a and b are prescribed, and P is the total (large-scale + convective) snowfall rate.

S2.2 In-cloud impaction scavenging

In cloud impaction scavenging is not treated in UKESM. In ECHAM-SALSA, in cloud impaction scavenging for liquid clouds is treated using the approach described in Croft et al. (2010), in which the impaction is presented as a function of particle size, wet median aerosol particle radius and cloud droplet radii. The fraction of activated particles is calculated as:

$$F_{i,imp,liq} = \Delta_m(r_{pg})\Delta t,$$
 (S2)

where $\Delta_m(r_{pg})$ is the mean mass scavenging coefficient (Holopainen et al., 2020). For ice clouds, ECHAM-SALSA assumes monodisperse ice crystals therefore there is no need to integrate over the whole ice crystal number distribution. The fraction of activated particles due to in cloud impaction scavenging for ice clouds is calculated as:

$$F_{i,imp,ice} = \pi R_{ice}^2 U_t(R_{ice}) E(R_{ice}, r_{pg}) ICNC\Delta t,$$
(S3)

where R_{ice} is the radius of the ice crystals at their maximum extent, U_t is the terminal velocity of the crystals, E is the collection efficiency for the collisions between aerosol particles and ice crystals and ICNC is the number concentration of the ice crystals (Croft et al., 2010; Holopainen et al., 2020).

S2.3 Nucleation scavenging/aerosol activation

In cloud nucleation scavenging for liquid clouds in UKESM1 is treated by the GLOMAP mode (Mann et al., 2010) based on Spracklen et al. (2005). In there, soluble particles with dry radius larger than 103 nm are assumed to act as cloud condensation nuclei, and insoluble-mode particles are scavenged only in cold environments with low enough temperatures (Mulcahy et al., 2020). The aerosols are then removed at the same rate as the cloud water is transformed to rain which is based on the large-scale precipitation scheme. The droplet activation itself follows Abdul-Razzak and Ghan (2000).

Updraughts (i.e., sub-grid scale vertical velocities, w) in UKESM1 are obtained by first estimating the sub-grid scale variability in vertical velocity by the probability density function (pdf)-based approach, which assumes a Gaussian distribution of vertical velocities across the gridbox with mean vertical velocity and standard deviation (σ_w) (Mulcahy et al., 2018; West et al., 2014). The number of activated droplets is calculated from the updraught-pdf, which has 20 equally spaced bins between $0 \le w \le 4 \sigma_w$. The σ_w is obtained from Eq. (1) following Ghan et al. (1997):

$$\sigma_w = \max\left(\sqrt{\frac{2}{3}TKE}, \sigma_{w(min)}\right) \tag{1}$$

where TKE is the turbulent kinetic energy and $\sigma_{w(min)}$ =0.01 m s⁻¹. The w is the derived from σ_w as in Fountoukis and Nenes (2005). Currently there is no representation of re-evaporation for falling droplets in UKESM1, thus no aerosols are released back to the atmosphere after they are wet scavenged. Removal via ice nucleation occurs by same rate as the riming rate of ice crystals aggregating in the cloud microphysics (Mulcahy et al., 2020).

In ECHAM-SALSA, in cloud nucleation scavenging for liquid clouds is based on the activation parameterisation presented in Abdul-Razzak and Ghan (2002). However, in SALSA2.0, this parameterisation is modified to account for the insoluble core in particles by adjusting the critical supersaturation calculations (Holopainen et al., 2020). To calculate the fraction of activated particles for ice clouds due to nucleation scavenging, the scavenging coefficients are derived from the scheme presented in Lohmann (2002). Only particles including mineral dust and black carbon are considered as ice nuclei. The calculations for in cloud nucleation scavenging fractions are presented in more detail in Holopainen et al. (2020). In ECHAM-SALSA, the sub-grid scale updraughts needed for activation are also based on TKE. They are derived from the average vertical velocities across the gridbox (large scale vertical velocity, w_L), to which the variability of the sub-grid scale vertical velocities (turbulent vertical velocity) is then added (Neubauer et al., 2019):

$$w = w_L + 0.7\sqrt{TKE} \tag{2}$$

Note that in contrast to UKESM1, in ECHAM-SALSA also particles noted as insoluble in Table S3 can activate as these are merely "less soluble" compared to the particles noted as soluble, which in turn, are "more soluble". Additionally, in ECHAM-SALSA, portion of the aerosols that are wet scavenged can re-evaporate back to the atmosphere (e.g., Stier et al., 2005). The coefficient for re-evaporation (between 0-1) is based on the amount of evaporated rain and snow and is used to multiply the scavenged aerosol mass mixing ratios thus releasing portion of the scavenged mass back to the atmosphere.

S2.4 Convective plume scavenging in UKESM1

In-cloud nucleation scavenging in convective clouds in UKESM1 is treated separately by convective plume scavenging scheme following the approach presented in Kipling et al. (2013). In this removal process, the aerosol mass and number mixing rations decrease in the rising convective plume via aerosol activating into cloud droplets within the convective updraught and falling out in the main precipitation shaft of the cumulonimbus. Particles in the soluble Aitken, accumulation and coarse mode are scavenged and the nucleation mode is not affected by this scheme. Additional details on why this separate scheme for nucleation scavenging for convective clouds was introduced can be found e.g. from Mulcahy et al. (2020).

S3 Utilised variables from the GCMs, data availability and average concentrations

Table S4 Summary of the variables utilized in this study from the GCMs. Note that PNSD refers to all the needed parameters to construct the full PNSD (see Sections 2.2 and 2.4.2 from the main text). 3D refers to variables that are vertically resolved in the GCMs, 2D refers to column integrated values and surface denotes variables available at the surface level. The variables are manually co-located to the HYSPLIT trajectories, except RH which is used as direct output from HYSPLIT.

Variable	3D, 2D (column integrated) or surface?	UKESM1	ECHAM-SALSA
PNSD ¹	3D	X	x
MMRs of OC/OM, BC and SO ₄ /H ₂ SO ₄	3D	X	x
Dry air density	3D	X	x
Total stratiform precipitation ²	surface	X	x
Total convective precipitation	surface	х	x
Sub-grid scale vertical velocity	3D	x, see Sect. S2.3	X
Number of activated particles	3D	х	x
Total precipitation ¹	surface	X	x
RH¹ (HYSPLIT)	3D	X	x
Cloud fraction	3D	X	x
Impaction scavenging (coef.)	2D	X	
Nucleation scavenging (coef.)	2D	X	
Plume scavenging (coef.)	2D	X	
Liquid stratiform precipitation	3D and surface	х	
SO ₂	3D	X	

¹also obtained for ECHAM-HAM, ECHAM-HAM-P3, CAM5 and NorESM to construct Figure 3 in the main text ²also obtained from ERA-Interim to represent observations

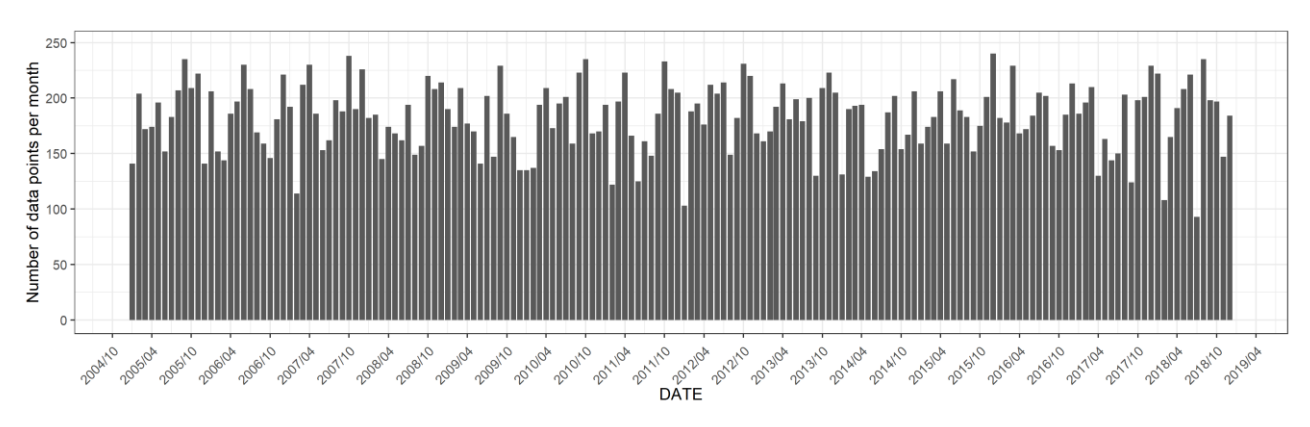


Figure S2 Number of available data rows in the particle size distribution measurements at SMEAR II for each month during the period between 2005 and 2018 for the temporally co-located DMPS observations and GCMs. With 3-hourly data, maximum number of data points per day is 8, thus single month can have 248 data rows at most (month length 31 days).

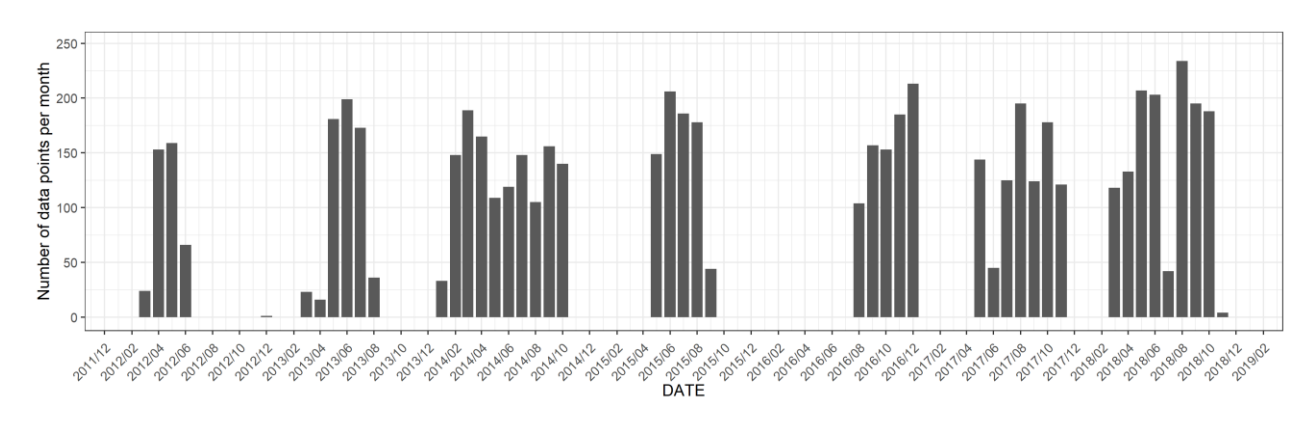


Figure S3 Number of available data rows in particle chemistry measurements at SMEAR II for each month during the period between 2012 and 2018 for the temporally co-located ACSM observations and GCMs. With 3-hourly data, maximum number of data points per day is 8, thus single month can have 248 data rows at most (month length 31 days).

Table S5 Median (25^{th} - 75^{th} percentiles) particle number concentrations (# cm⁻³) at SMEAR II between 2005 and 2018 for nucleation ($d_p < 10$ nm), Aitken ($d_p = 10$ -100 nm) and accumulation ($d_p > 100$ nm) mode particles for the temporally co-located data. The number concentrations for each mode are calculated from the PNSDs (see Section 2.4.2 on the main text how the PNSDs were obtained for the GCMs).

	Mode	MAM/spring	JJA/summer	SON/autumn	DJF/winter		
DMPS	Nucleation	49.6 (15.8-158)	24.0 (8.79-57.4)	24.0 (8.79-57.4) 34.0 (11.6-87.2)			
measurements	Aitken	1311 (753-2253)	1182 (766-1863)	868 (470-1503)	572 (332-992)		
	Accumulation	352 (168-609)	552 (329-836)	237 (125-449)	259 (135-454)		
UKESM1	Nucleation	0.962 (0.118-	0.0304 (0.0029-	0.366 (0.0495-	1.95 (0.543-		
		5.52)	0.4300)	1.70)	5.22)		
	Aitken	405 (240-620)	167 (88.4-280) 296 (154-449)		422 (280-620)		
	Accumulation	367 (233-557)	340 (209-493)	298 (180-466)	368 (234-566)		
ECHAM-	Nucleation	40.8 (13.0-132)	24.9 (7.17-84.0)	30.3 (8.13-102)	8.01 (3.28-20.1)		
SALSA	Aitken	792 (506-1165)	909 (654-1263)	725 (458-1046)	736 (447-1183)		
	Accumulation	175 (95.3-342)	378 (252-565)	197 (103-368)	221 (121-449)		

Table S6 Median (25th-75th percentiles) total mass concentrations ($\mu g \ m^{-3}$) for sub-micron OA, SO₄ and BC between 2012 and 2018 at SMEAR II for the temporally co-located data.

	Aerosol	MAM/spring	JJA/summer	SON/autumn	DJF/winter
	species				
Chemistry	OA	1.33 (0.637-2.42)	2.20 (1.26-3.63)	1.01 (0.534-1.98)	0.809 (0.462-1.52)
measurements	SO ₄	0.343 (0.190-0.613)	0.386 (0.230-0.689)	0.298 (0.119-0.868)	0.521 (0.205-1.08)
	BC	0.139 (0.074-0.238)	0.148 (0.081-0.246)	0.154 (0.076-0.310)	0.188 (0.103-0.370)
UKESM1	OA	0.976 (0.672-1.54)	2.00 (1.25-3.32)	0.874 (0.549-1.49)	0.746 (0.488-1.15)
	SO ₄	0.495 (0.352-0.729)	0.423 (0.312-0.618)	0.333 (0.201-0.629)	0.325 (0.203-0.712)
	BC	0.075 (0.044-0.126)	0.070 (0.038-0.115)	0.080 (0.046-0.133)	0.118 (0.070-0.185)
ECHAM-	OA	0.627 (0.371-1.01)	1.30 (0.861-1.96)	0.725 (0.350-1.29)	0.775 (0.414-1.46)
SALSA	SO ₄	0.403 (0.211-0.721)	0.492 (0.288-0.769)	0.349 (0.160-0.934)	0.319 (0.147-0.605)
	BC	0.085 (0.050-0.146)	0.066 (0.039-0.113)	0.084 (0.047-0.169)	0.125 (0.069-0.244)

S4 Representability of UKESM1 and ECHAM-SALSA amongst larger group of GCMs

The representativity of UKESM1 and ECHAM-SALSA compared to a larger group of GCMs from the AeroCom cohort (simulation years 2009-2013) was assessed. All the model simulations followed AMIP style runs following the experiment setup for AeroCom phase III GCMTraj experiment (see also Aerosol GCM Trajectory (GCMTraj) | AeroCom, 2024). Therefore, only summaries of the models are given here in Sect S4.1-S.4.5.

For the comparison on relation to the aerosol—precipitation relationships, the particle size distribution variables and total precipitation (see Table S4) were inspected. From the aerosol variables the full particle number size distributions were calculated in a similar manner as for UKESM1 (see Sect. 2.4.2), followed by integration to obtain total mass and number concentrations for each model. Figure S4 shows the normalized particle mass and number concentrations as a function of the accumulated total precipitation (Figure S4a-b), the sample size (Figure S4c) for each precipitation bin and the mean rainfall rates along the trajectories (Figure S4d) for each of the GCMs. For normalized aerosol mass, all the GCMs except NorESM exhibit relatively similar behaviour up to 5 mm of accumulated precipitation. For normalized aerosol number, the differences between the models are larger. NorESM has very strong initial decrease for both particle mass and number, which starts exhibiting increase for both with increasing accumulated precipitation after ~5 mm of accumulated precipitation. The average rainfall rates between the GCMs (Figure S4d) are relatively close to each other. CAM5 and NorESM exhibit slightly smaller rates, whereas UKESM1 and the three ECHAM models, ECHAM-SALSA, ECHAM-HAM and ECHAM-HAM-P3, exhibit slightly higher rates. Overall, neither UKESM1 nor ECHAM-SALSA are presenting the extremes, i.e., they are relatively close to the GCM ensemble mean (not shown) when representing the aerosol-accumulated precipitation relationships. Therefore, these GCMs are good examples amongst this larger group of GCMs.

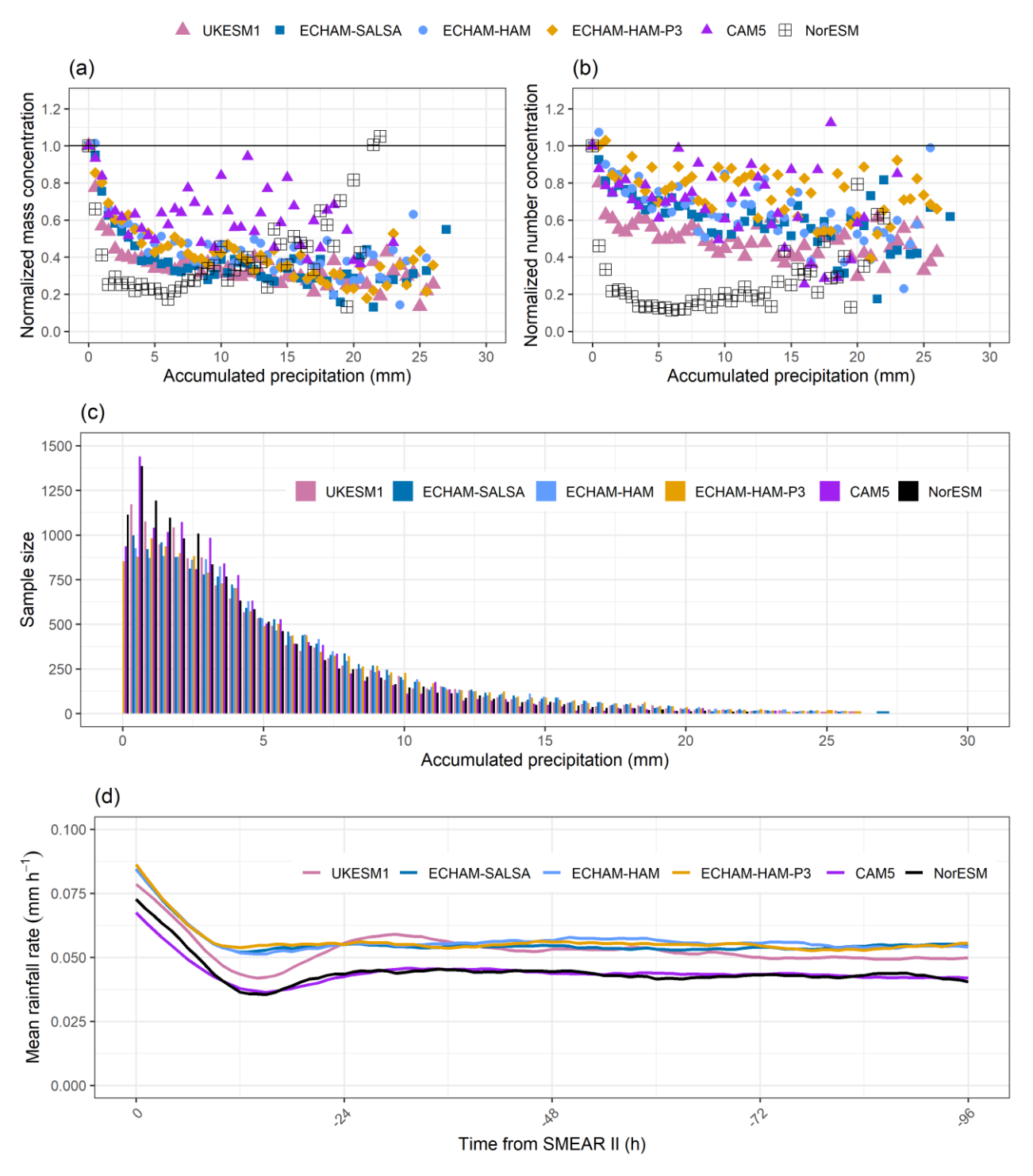


Figure S4 Normalized total particle mass (a) and number (b) concentration at SMEAR II as a function of accumulated total (stratiform and convective, including both liquid rain and snow) precipitation along the 96-h long air mass trajectories for the different GCMs. The coloured points in (a) and (b) show the median values for each 0.5 mm bin of accumulated precipitation when the number of trajectories in the bin was 10 or larger. The sample size for the corresponding 0.5 mm bins is shown in (c) and the average rainfall rates along the trajectories are shown in (d). The shown data have been temporally harmonized within the GCMs, thus including data between 2009 and 2013.

S4.1 ECHAM-HAM

ECHAM6.3-HAM2.3 (referred as ECHAM-HAM) is a global aerosol-climate model consisting of ECHAM (Stevens et al., 2013) coupled with the Hamburg Aerosol Model HAM (Tegen et al., 2019). In difference to ECHAM-SALSA, ECHAM-HAM uses the modal aerosol model M7 as its microphysical core (Stier et al., 2005; Vignati et al., 2004).

ECHAM-HAM is run at a horizontal resolution corresponding approximately to 1.875° x 1.875° (latitude-longitude) and 47 vertical levels extending up to 0.01 hPa.

M7 has four log-normal modes for soluble (nucleation, Aitken, accumulation, coarse) and three for insoluble (Aitken, accumulation, coarse) aerosol particles. Sulfate is included in all seven modes, black carbon and primary organic aerosol in all modes except the nucleation mode and insoluble accumulation and coarse modes. Sea salt and mineral dust are traced in soluble accumulation and coarse mode and mineral dust also in insoluble accumulation and coarse mode.

The wet scavenging schemes in ECHAM-HAM are relatively similar to ECHAM-SALSA (see Sect. S2). In-cloud impaction scavenging is dependent on the wet particle size and follows Croft et al. (2010) and scavenging via droplet activation, which follows Abdul-Razzak and Ghan (2000). The in-cloud scavenging scheme considers scavenging in different cloud types, distinguishing between stratiform and convective clouds and warm, cold, and mixed-phase clouds. Below clouds particles are scavenged by rain and snow using a size-dependent below-cloud scavenging scheme (Croft et al., 2009). Scavenged particles can also be resuspended in the atmosphere, as in ECHAM-SALSA, when precipitation evaporates (Stier et al., 2005).

S4.2 ECHAM-HAM-P3

ECHAM6.3-HAM2.3-P3 (referred as ECHAM-HAM-P3) is the combination of the ECHAM (Stevens et al., 2013), the Hamburg Aerosol Module (Tegen et al., 2019) and Perturbed Particle Physics (P3) ice cloud microphysics scheme (Dietlicher et al., 2018, 2019). The P3 configuration of ECHAM-HAM offers better-constrained conversion rates and prognostic ice sedimentation, as well as a more realistic representation of mixed-phase and cirrus cloud cover (Dietlicher et al., 2019). The simulations were run with a horizontal resolution of 1.875° x 1.875° (latitude-longitude) and with 47 vertical levels extending up to a 0.01 hPa.

Description of aerosols and wet scavenging processes in ECHAM-HAM-P3 are identical to ECHAM-HAM.

S4.3 CAM5

The Community Atmosphere Model version 5.3 (CAM5.3, hereafter only CAM5, see also Neale et al., 2012) is the atmospheric component of the Community Earth System Model (CESM, Hurrell et al., 2013). CAM5 is configured with at a spatial resolution of 1.9°x2.5° (latitude-longitude), and 30 vertical layers from the surface to 3.6 hPa (corresponding approximately to 40 km).

The aerosols in CAM5 (Liu et al., 2016) are distributed to four lognormal modes (i.e., Aitken, accumulation, coarse, and primary carbon modes). The model predicts aerosol species including sulfate, black carbon, primary organic matter, secondary organic aerosol, mineral dust, and sea salt.

The aerosol wet scavenging and convective transport in the model are improved based on Wang et al., (2013) on top of the default CAM5.

S.4.4 NorESM

The Norwegian Earth System Model intermediate version (NorESM1.2; Kirkevåg et al., 2018) is based on version 1.2 of the CESM (Hurrell et al., 2013) and uses the atmospheric model CAM5.3-Oslo. CAM5.5-Oslo is an updated version of the Community Atmospheric Model version CAM5.3 (Liu et al., 2016; Neale et al., 2012). The ocean, land, and sea-ice models used are the Bergen version of the Miami Isopycnic Co-ordinate Ocean Model (MICOM) (Bentsen et al., 2013),

Community Land Model (CLM) 4.5 and CICE4 respectively. The model has 30 vertical levels and has a horizontal resolution of 1.9° x 1.25° (latitude-longitude).

CAM5.3-Oslo has its own aerosol module, OsloAero (Kirkevåg et al., 2018), which has 21 aerosol tracers distributed among six species. These species include sulfate, secondary organic aerosol, black carbon, organic matter, mineral dust and sea salt. OsloAero also includes a general chemical solver (CAM-Chem) and a standardized chemical code preprocessor (MOZART; Emmons et al., 2010).

Wet scavenging includes in-cloud scavenging (formation of cloud droplets by impaction and nucleation) and below-cloud scavenging (wet removal of aerosols by precipitation) (Kirkevåg et al., 2018). The aerosol activation scheme follows Abdul-Razzak and Ghan (2000).

S5 Additional figures and tables supporting the main results

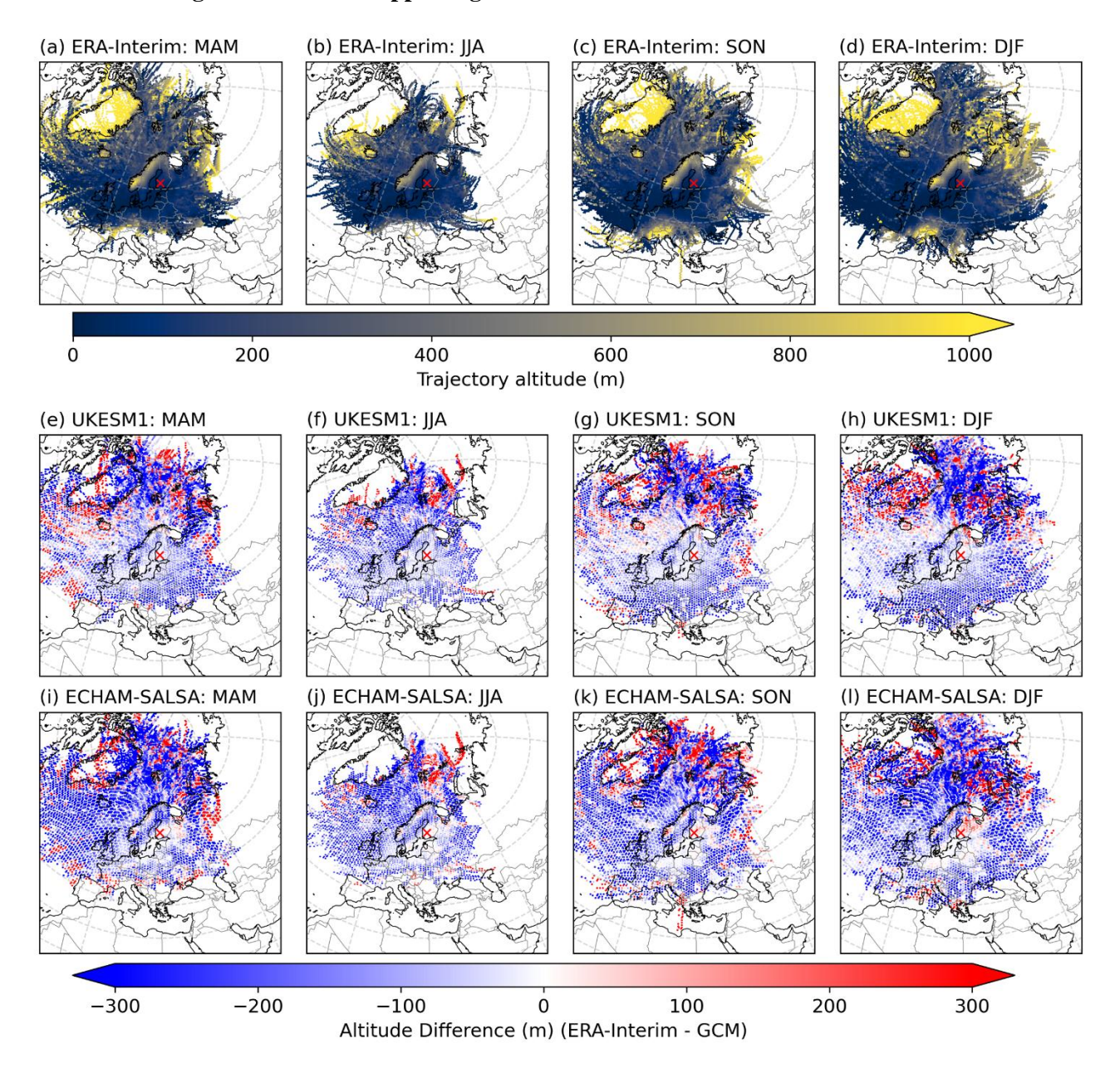


Figure S5 ERA-Interim air mass trajectory altitudes (means for each hexagonal grid with grid resolution of 150 in the x-direction) for spring (MAM), summer (JJA), autumn (SON) and winter (DJF) are shown in the top row. The altitudes for UKESM1 (e-h) and ECHAM-SALSA (i-l) are shown as differences to the ERA-Interim altitudes. Before calculating the differences, the GCM hexagonal grids were first regridded to match the gridding in ERA-Interim. Red cross shows the location of SMEAR II.

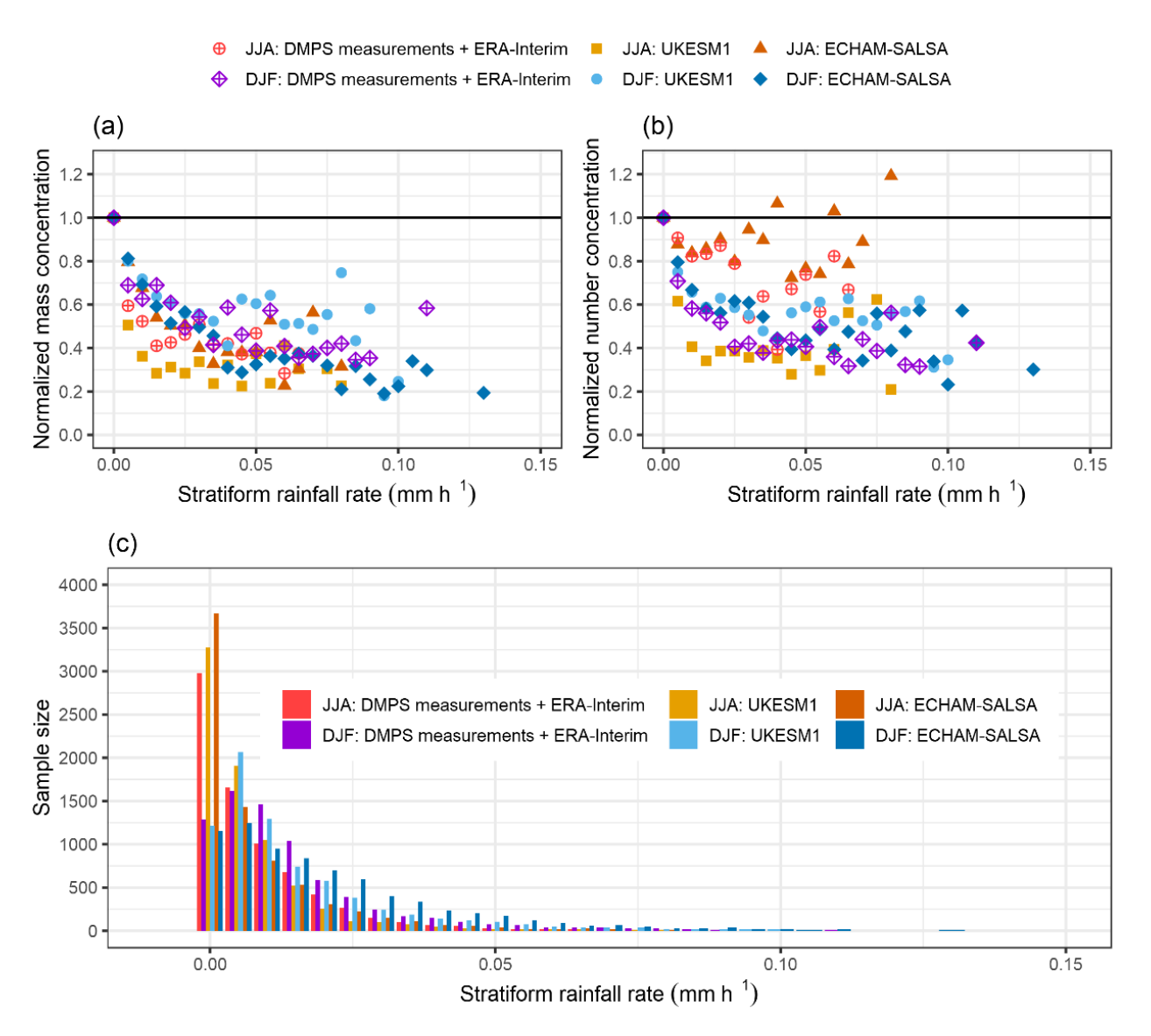


Figure S6 Normalized total (d_p = 3-1000 nm) particle mass (a) and number (b) at SMEAR II for summer (JJA) and wintertime (DJF) as a function average experienced stratiform rainfall rate at the surface (median values over the along the 96-h long air mass trajectories) for observations (DMPS measurements paired with ERA-Interim trajectories) and GCMs (UKESM and SALSA). The coloured points show the median values for each 0.005 mm/ bin of stratiform rainfall rate when the number of data rows in the bin was 10 or larger. The sample size for each corresponding bin is shown in (c).

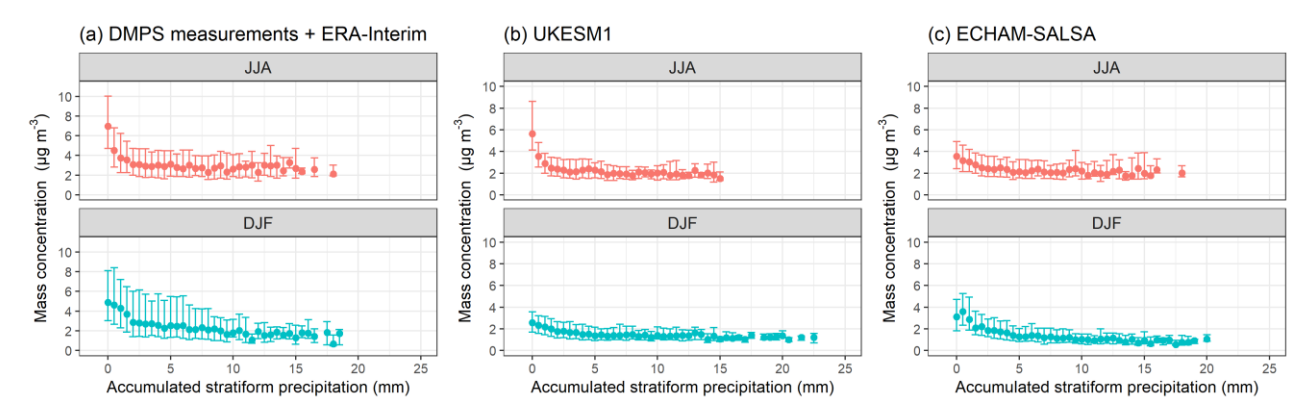


Figure S7 Total submicron particle mass ($\rho=1.6~g~cm^{-3}$) concentration at SMEAR II as a function of 0-25 mm of accumulated stratiform surface precipitation along the 96-h long air mass trajectories for (a) SMEAR II + ERA-Interim, (b) UKESM1 and (c) ECHAM-SALSA for summer (JJA) and winter (DJF). The points show the median values for each 0.5 mm bin of accumulated precipitation when the number of data rows for the bin was 10 or larger and the bars show the $25^{th}-75^{th}$ percentiles.

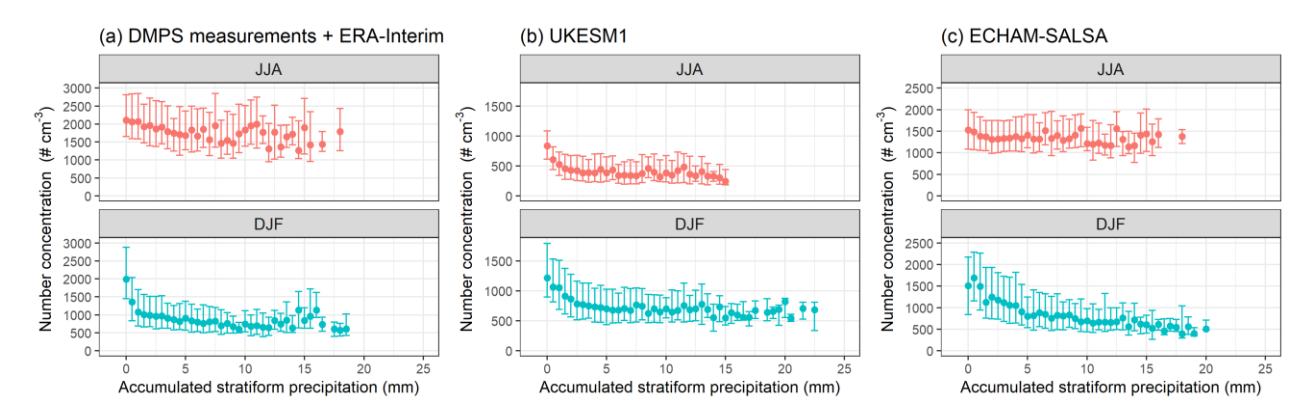


Figure S8 Total submicron particle number concentration at SMEAR II as a function of 0-25 mm of accumulated stratiform surface precipitation along the 96-h long air mass trajectories for (a) SMEAR II + ERA-Interim, (b) UKESM1 and (c) ECHAM-SALSA for summer (JJA) and winter (DJF). The points show the median values for each 0.5 mm bin of accumulated precipitation when the number of data rows for the bin was 10 or larger and the bars show the $25^{th} - 75^{th}$ percentiles. Note the different y-axis range for each approach.

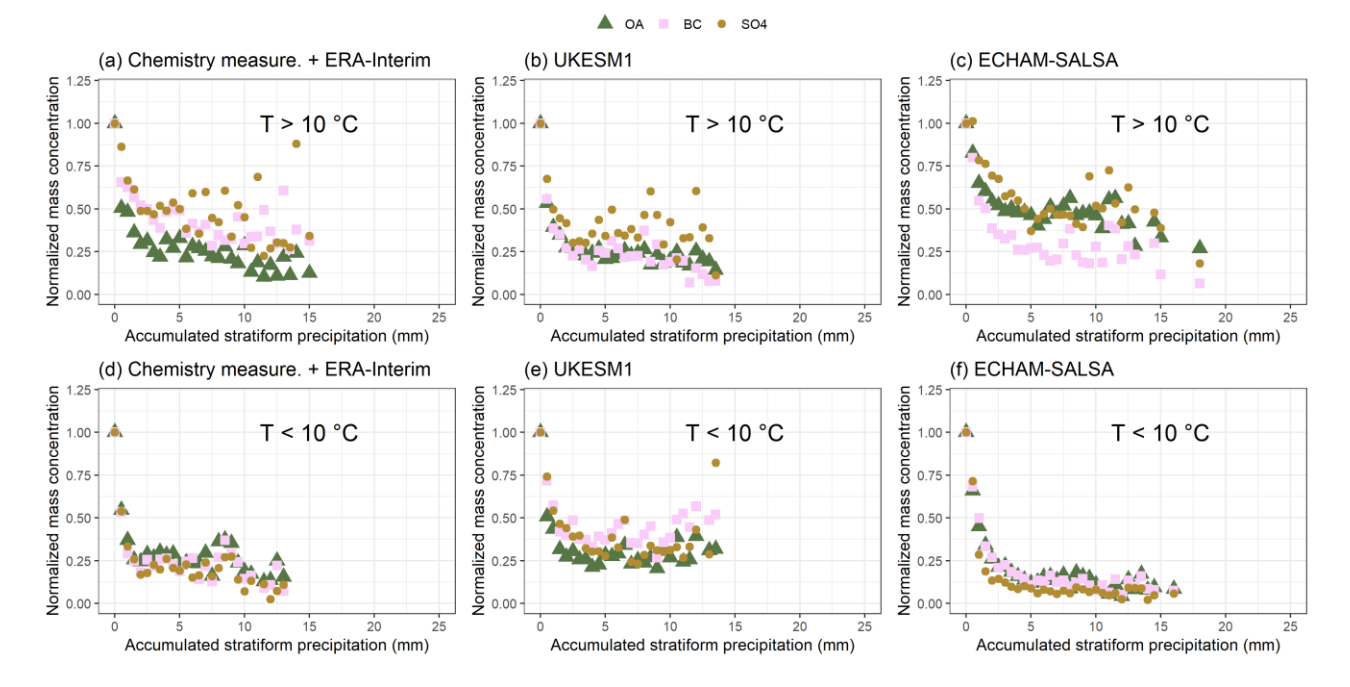


Figure S9 Normalized mass concentrations of submicron OA, BC and SO4 for (a) chemistry measurements paired with ERA-Interim trajectories, (b) UKESM1 and (c) ECHAM-SALSA at SMEAR II as a function of 0-25 mm of accumulated stratiform surface precipitation along the 96-h long air mass trajectories for warm (T > 10 C, top row) and cold (T < 10 C, bottom row) months. The coloured points show the normalized median values for each 0.5 mm bin of accumulated precipitation when the number of data rows for the bin was 10 or larger.

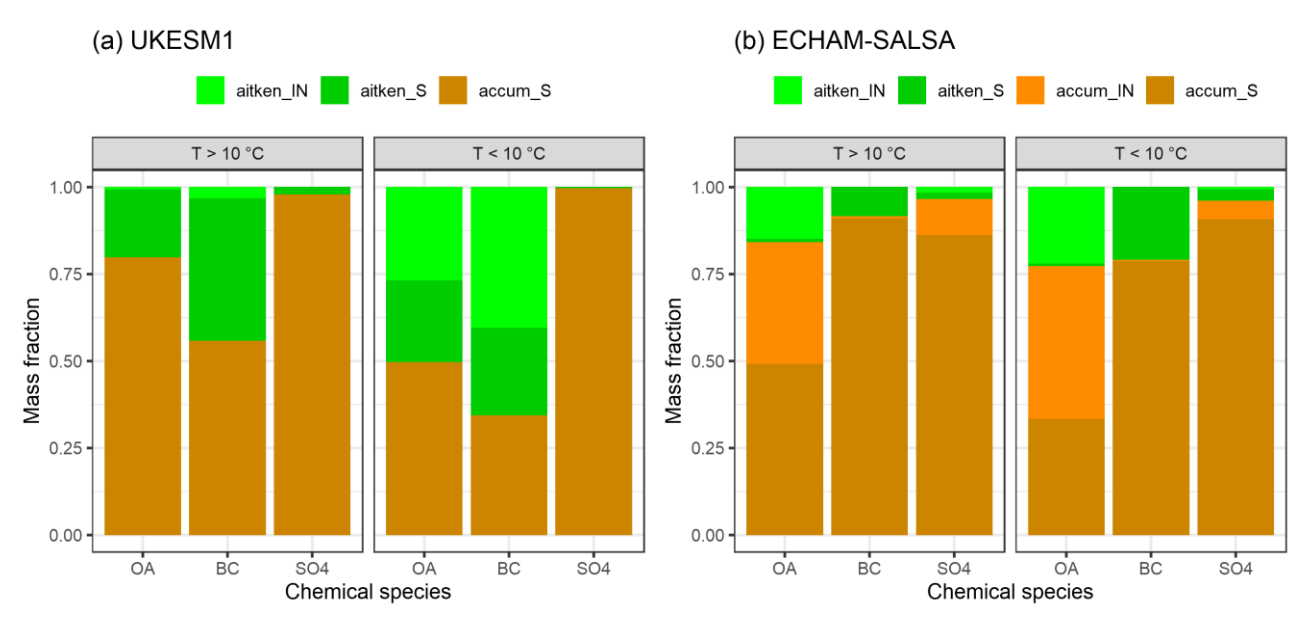


Figure S10 Size segregated chemical composition (derived from median mass concentrations) of the particles at SMEAR II from UKESM1 and ECHAM-SALSA following the seasonal division based on temperature. The suffixes within the legend refer to insoluble (IN) and soluble (S) particle modes. The sectional bins from ECHAM-SALSA are assigned into Aitken (bins ranging from 19.6 nm to 97.6 nm) and accumulation (bins ranging from 97.6 nm to 700 nm) classes for easier comparison to UKESM1.

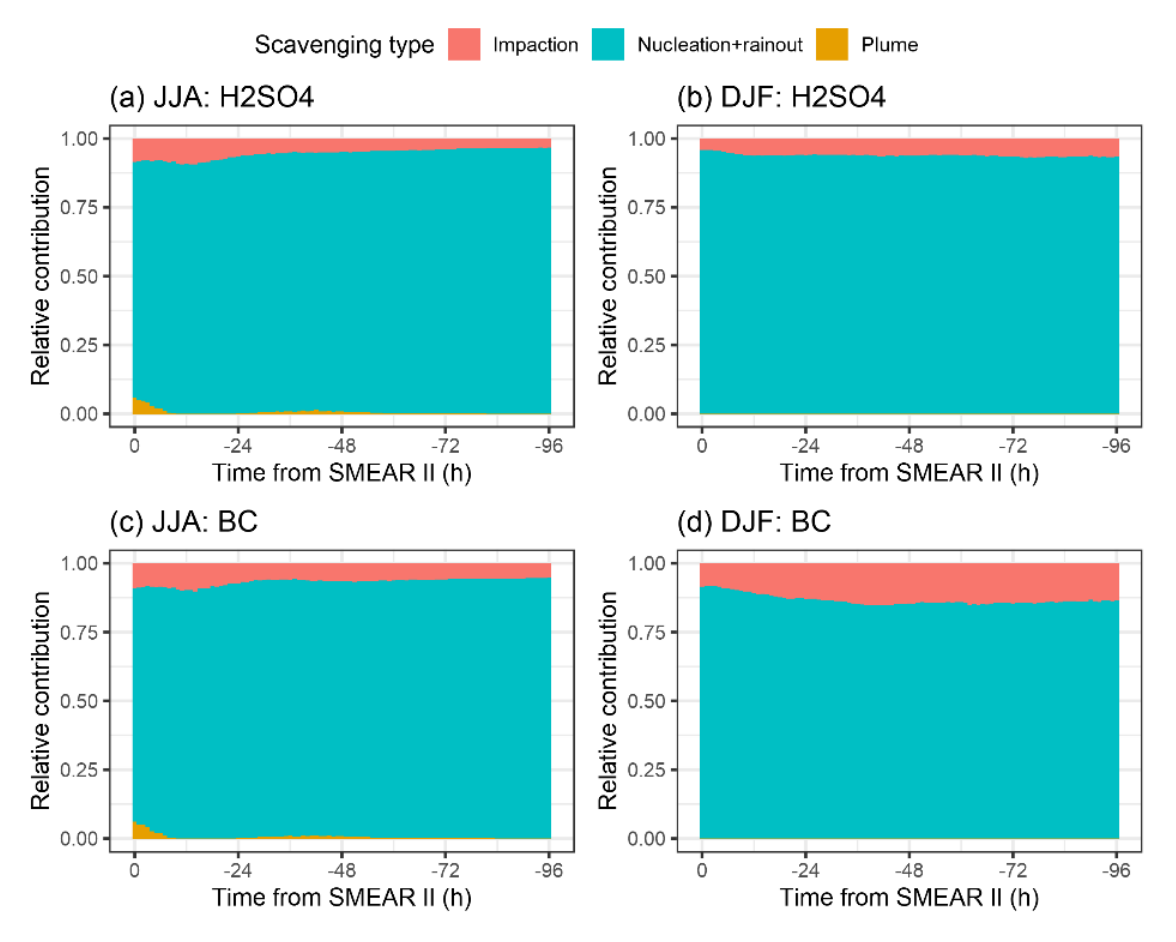


Figure S11 Relative contributions of the different removal pathways in UKESM1 for H_2SO_4 in (a)-(b) and BC in (c)-(d) as a function of time from SMEAR II. Impaction refers to the below-cloud impaction scavenging, nucleation+rainout describes the activation process followed by removal of the particles via the formed raindrops and plume scavenging is the removal due to convective clouds.

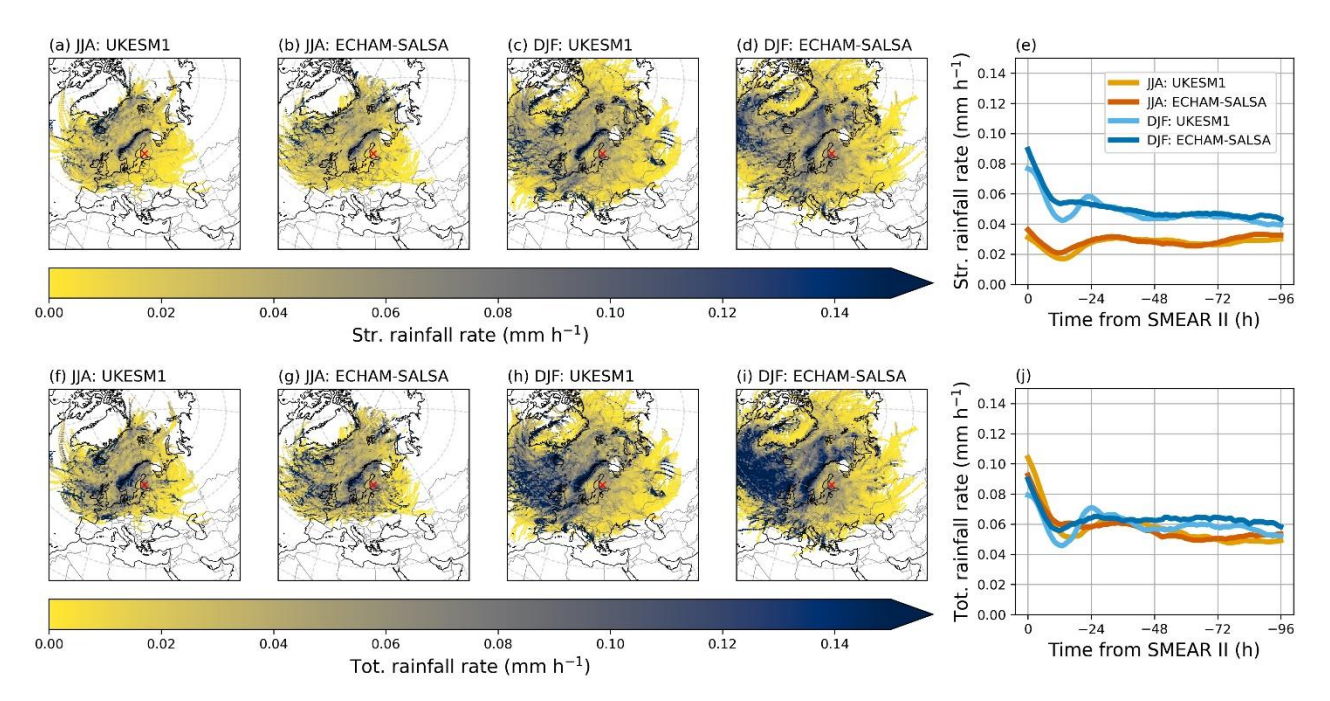


Figure S12 The evolution of the stratiform rainfall rate (mm h^{-1}) is presented in the top row, and the bottom row displays total (stratiform + convective) rainfall rate (mm h^{-1}). For the maps, means are calculated for each hexagonal gridbox (grid resolution being 150 in the x direction) that the trajectory crosses, and for the rightmost panels, means have been calculated for each hour along the trajectory.

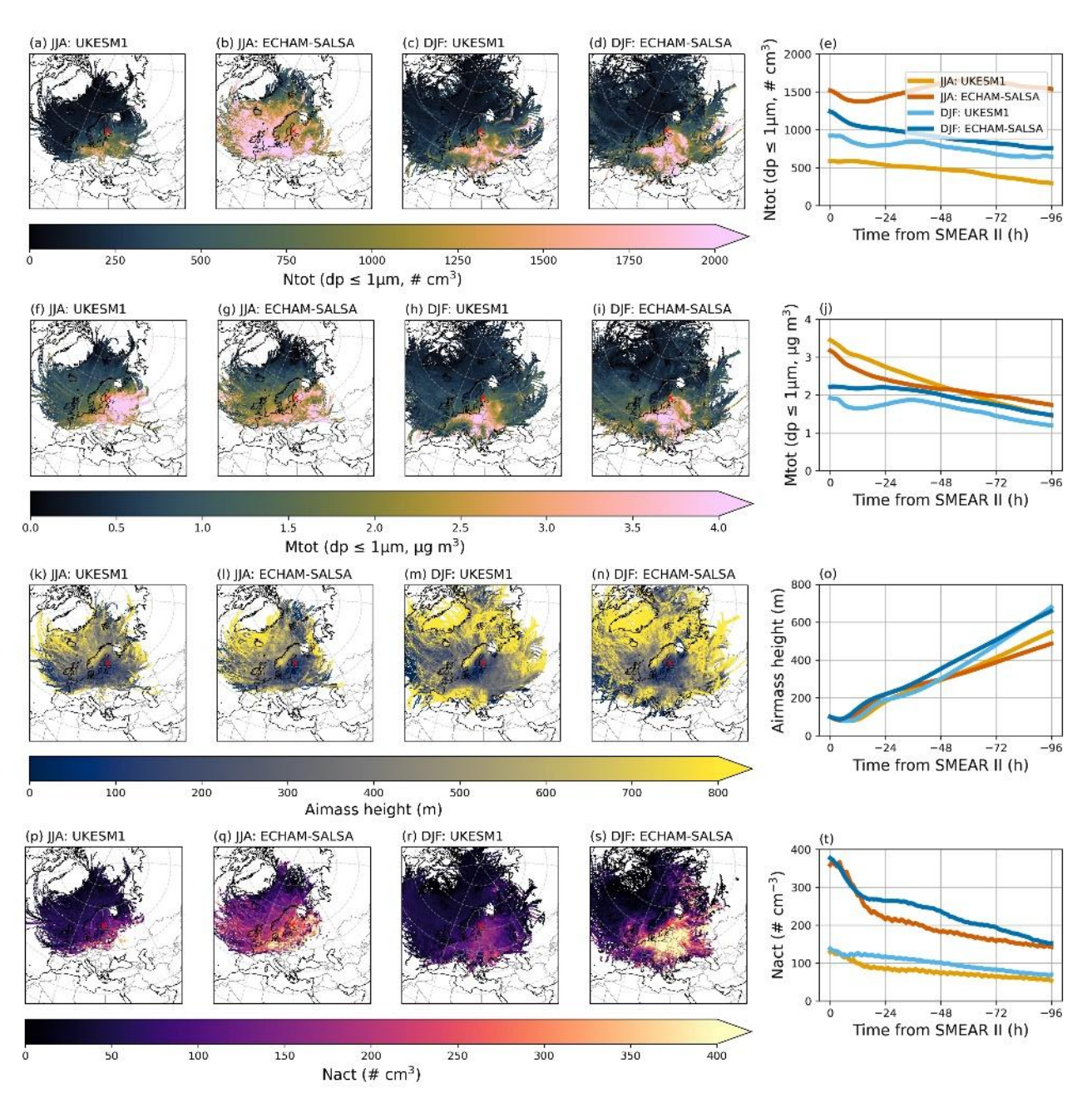


Figure S13 The evolution of the total particle number (N_{tot} , top row), total particle mass (M_{tot} , second row), the air mass height (third row) and number of activated particles (N_{act} , bottom row) along the trajectories. For the maps, means are calculated for each hexagonal gridbox (grid resolution being 150 in the x-direction) that the trajectory crosses, and for the rightmost panels, means have been calculated for each hour along the trajectory. Note that N_{act} also include coarse mode aerosols, and it only shows cases when the air mass is in-cloud.

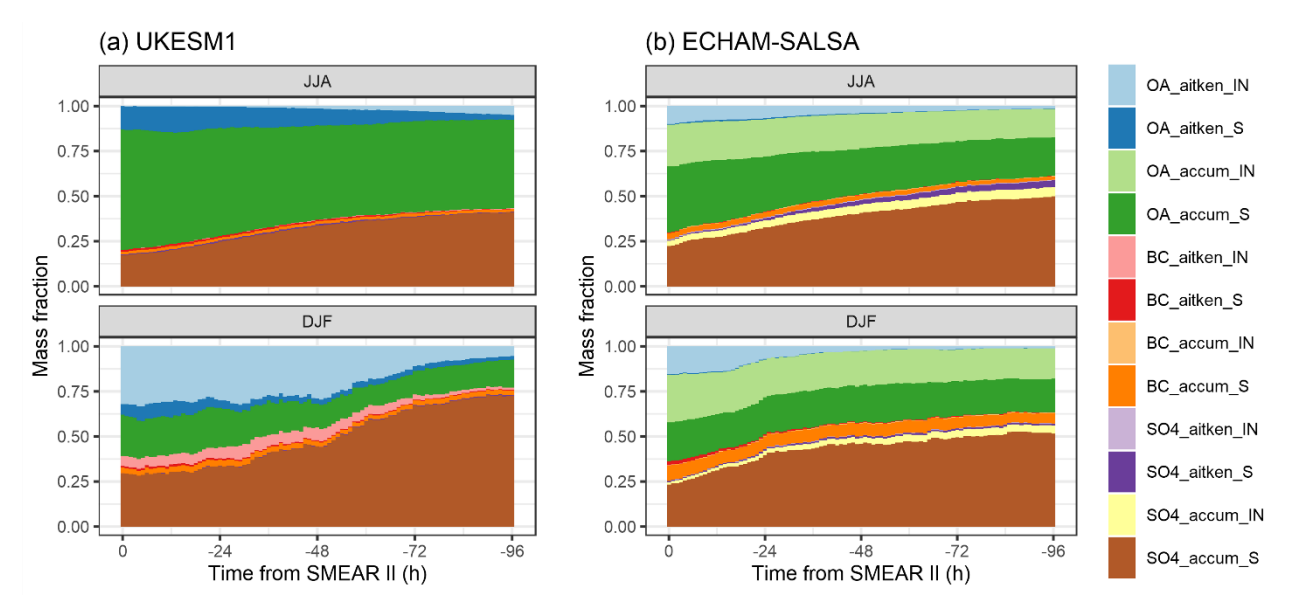


Figure S14 Size resolved chemical composition of particle mass concentration for Aitken and accumulation models as a function of time from SMEAR II (h) for (a) UKESM1 and (b) ECHAM-SALSA. The fractions are derived from median mass concentrations for each hour along the trajectory. The suffixes within the legend refer to insoluble (IN) and soluble (S) particle modes. The sectional bins from ECHAM-SALSA are assigned into Aitken (bins ranging from 19.6 nm to 97.6 nm) and accumulation (bins ranging from 97.6 nm to 700 nm) classes for easier comparison to UKESM1 (see also Table S3). Note that some modes are not present in both GCMs.

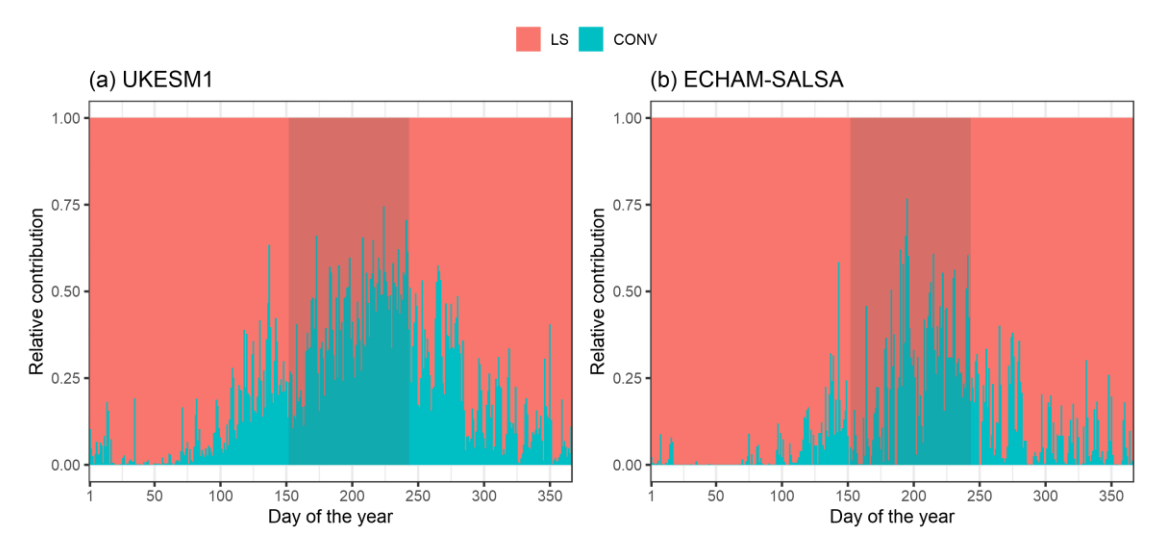


Figure S15 Relative contribution accumulated stratiform (LS) and convective (CONV) precipitation as a function of the day of the year for (a) UKESM1 and (b) ECHAM-SALSA. The shaded area indicates the days included in summer/JJA. The relative contribution is calculated from the median values of accumulated precipitation over the 96-hour long trajectories.

Table S7 Definitions for the classification exploited in Section 5 in the main text.

Group id in Isokääntä et al. (2022)	Notation used in this study	History during the last 0-24 h before arrival to SMEAR II	Quick summary
1	clear sky	Air mass has not experienced precipitation or RH > 94 %	No precipitation or in-cloud processing
3	in-cloud	Air mass has experienced RH > 94 % but not precipitation	in-cloud processing only

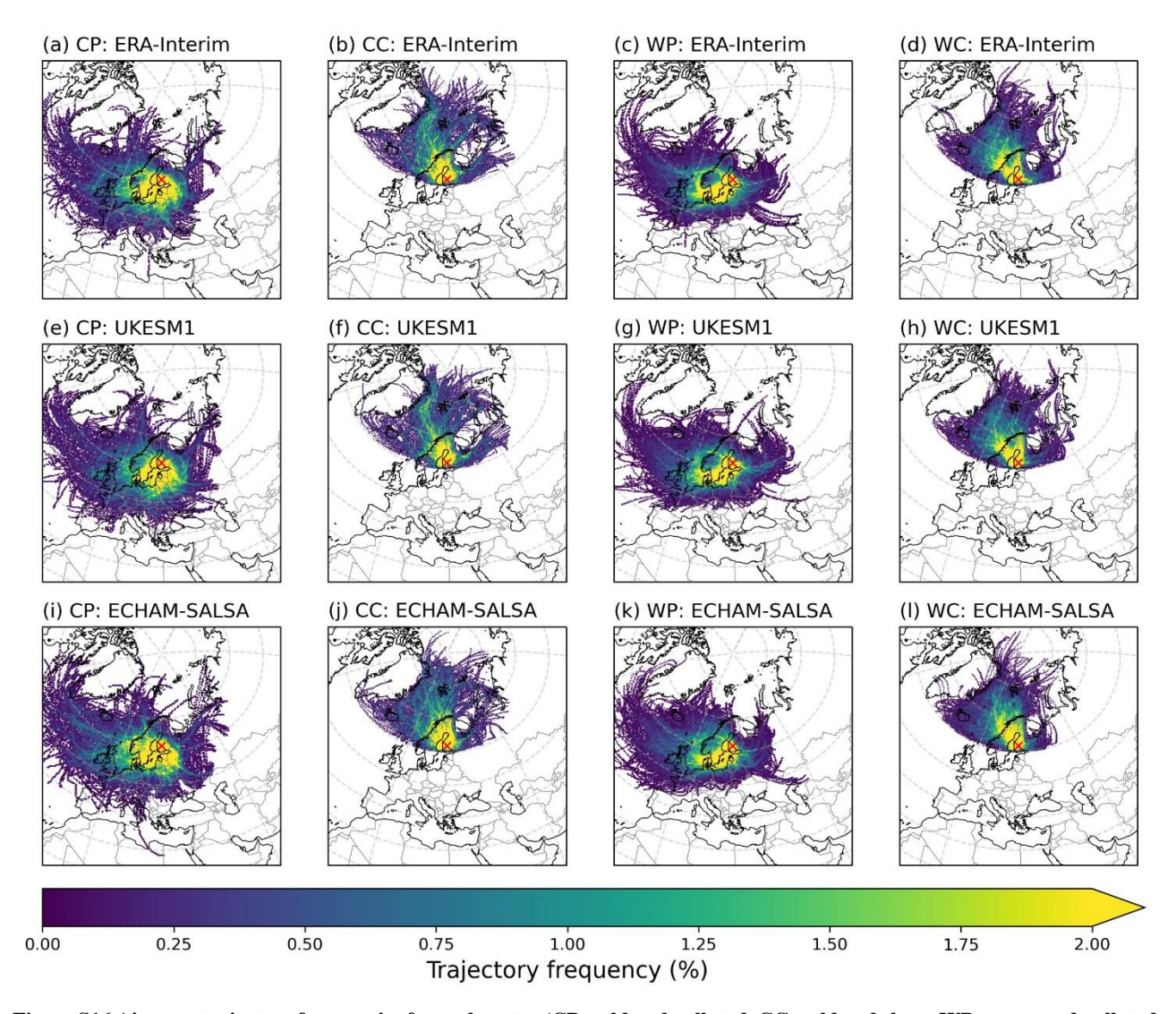


Figure S16 Air mass trajectory frequencies for each sector (CP: cold and polluted, CC: cold and clean, WP: warm and polluted, WC: warm and clean) for temporally co-located data from 2012-2018. Red cross shows the location of SMEAR II. ERA-Interim is presented in (a)-(d), UKESM1 in (e)-(h) and ECHAM-SALSA in (i)-(l).

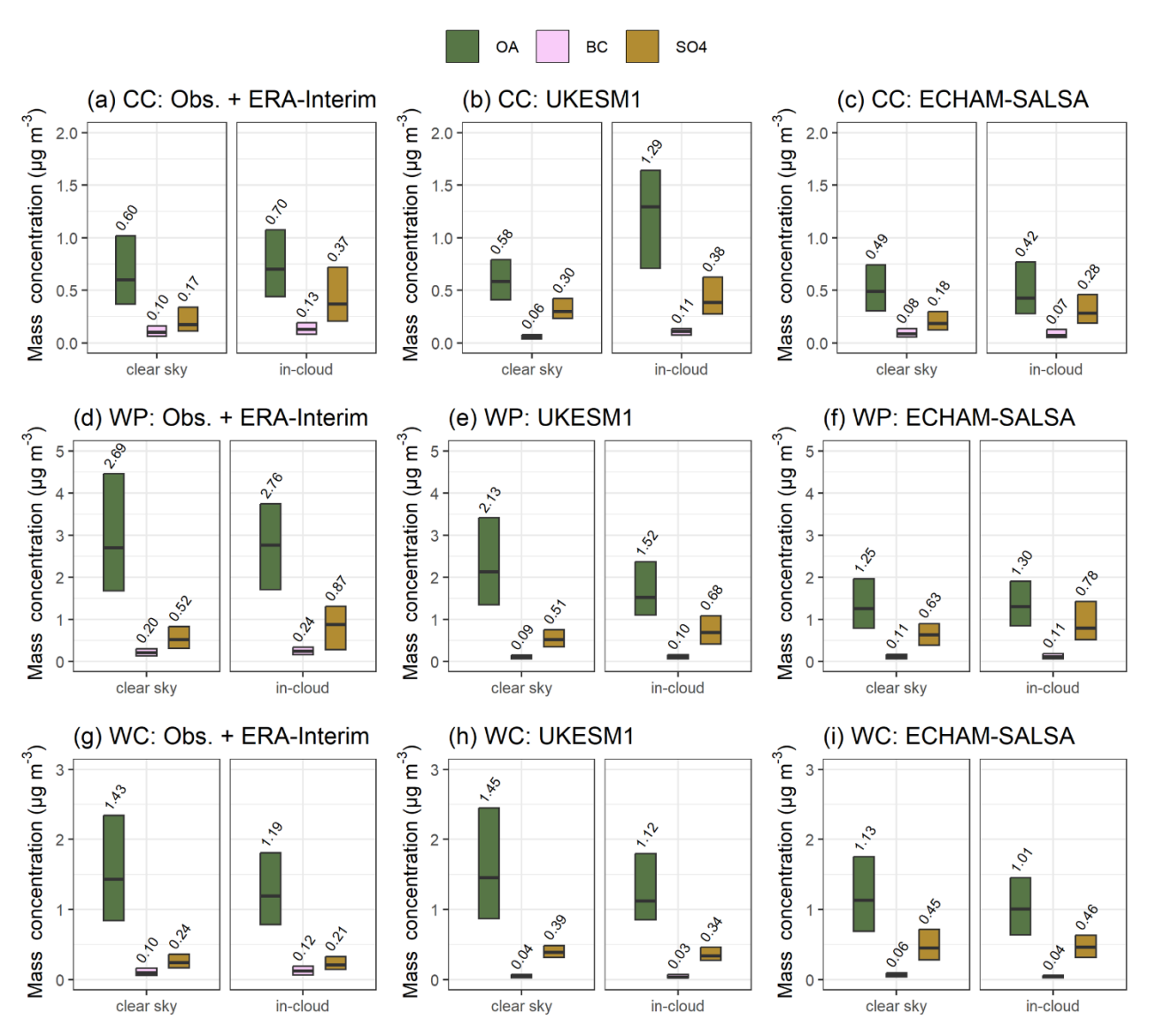


Figure S17 Median (black horizontal lines and numerical values) particle mass concentrations with 25th-75th percentiles (boxes) for OA, BC, and SO4 for rest of the air mass sectors: CC-cold and clean, WP-warm and polluted and WC-warm and clean. The experienced conditions by the air mass are denoted as clear sky and in-cloud (non-precipitating) (described in Table S7).

Table S8 Statistical significance (p-values) of the differences between the data from clear sky and in-cloud groups (based on RH-derived cloud proxy) for OA, BC and SO₄ for each sector for observational approach (OBS) and the GCMs (UKESM and SALSA). P-values were obtained by Kruskal-Wallis rank sum test. Values smaller than 0.01 (or 0.05, depending on source literature) indicate the null hypothesis (distributions are identical) could be rejected.

	Sector											
Species	CP: Cold and polluted			CC: Cold and clean		WP: Warm and polluted			WC: Warm and clean			
	OBS	UKESM	SALSA	OBS	UKESM	SALSA	OBS	UKESM	SALSA	OBS	UKESM	SALSA
OA	0.004	< 0.001	< 0.001	0.041	< 0.001	0.270	0.360	< 0.001	0.361	0.038	0.030	0.005
SO4	0.001	< 0.001	< 0.001	< 0.001	0.001	< 0.001	< 0.001	< 0.001	< 0.001	0.140	0.189	0.629
BC	0.491	< 0.001	< 0.001	< 0.001	< 0.001	0.041	0.014	0.345	0.101	0.034	0.347	< 0.001

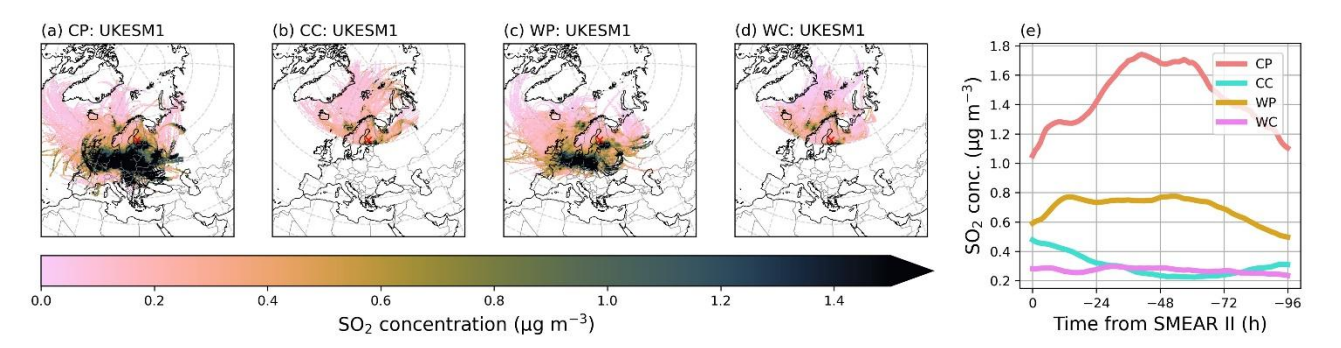


Figure S18 SO₂ concentrations along the air mass trajectories from UKESM1. For the maps, means are calculated for each hexagonal gridbox (grid resolution being 150 in the x-direction) that the trajectory crosses, and for the rightmost panels, means have been calculated for each hour along the trajectory.

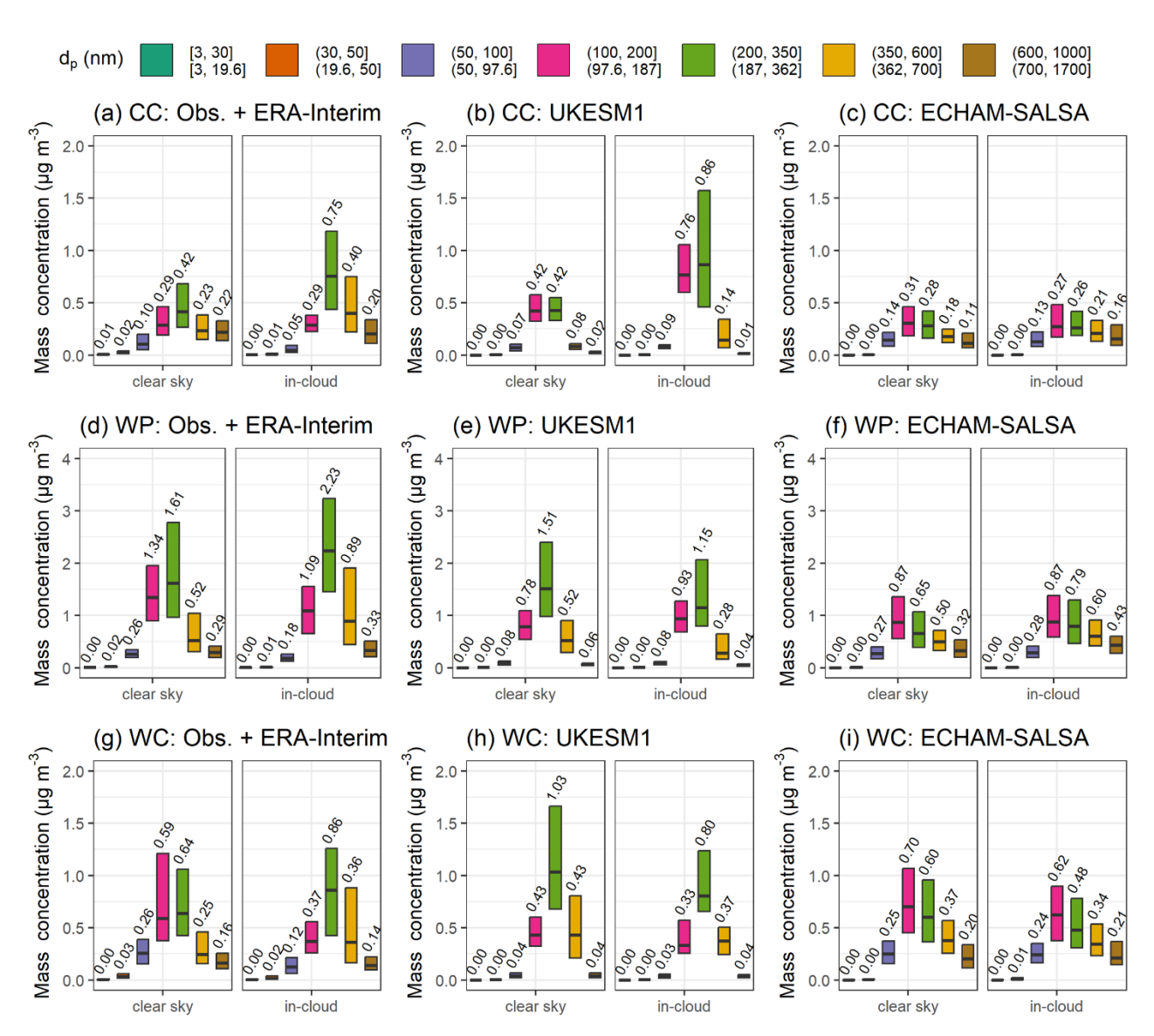


Figure S19 Median (black horizontal lines and numerical values) particle mass concentrations with 25th–75th percentiles (boxes) for selected size bins for the rest of the air mass sectors: CC-cold and clean, WP-warm and polluted and WC-warm and clean. For ECHAM-SALSA, the native size bins are shown (bottom row of the legend). The experienced conditions by the air mass are denoted as clear sky and in-cloud (non-precipitating). The data for the observations here is reduced due to the temporal co-location with the GCMs (see Section 2.4 from the main text), thus some differences to Isokääntä et al., (2022) are expected

Table S9 Statistical significance (p-values) of the differences between the data from clear sky and in-cloud groups (based on RH-derived cloud proxy) for aerosol size classes for each sector for the GCMs (UKESM and SALSA). P-values were obtained by Kruskal-Wallis rank sum test. Values smaller than 0.01 (or 0.05, depending on source literature) indicate the null hypothesis (distributions are identical) could be rejected.

	Sector										
Size class	CP: Cold a	nd polluted	CC: Cold and clean		WP: Warm	and polluted	WC: Warm and clean				
-	UKESM	SALSA	UKESM	SALSA	UKESM	SALSA	UKESM	SALSA			
[3, 30]	0.003	< 0.001	0.274	0.005	0.204	0.257	0.501	< 0.001			
(3, 50]	0.295	0.002	0.407	0.838	0.731	0.991	0.232	< 0.001			
(50, 100]	0.329	< 0.001	0.338	0.337	0.958	0.100	0.079	0.366			
(100, 200]	< 0.001	< 0.001	< 0.001	0.537	0.011	0.266	0.024	0.001			
(200, 350]	< 0.001	< 0.001	< 0.001	0.961	0.001	0.006	0.085	< 0.001			
(350, 600]	0.004	< 0.001	< 0.001	0.010	< 0.001	< 0.001	0.075	0.065			
(600, 1000]	0.555	< 0.001	0.005	0.001	< 0.001	< 0.001	0.452	0.368			

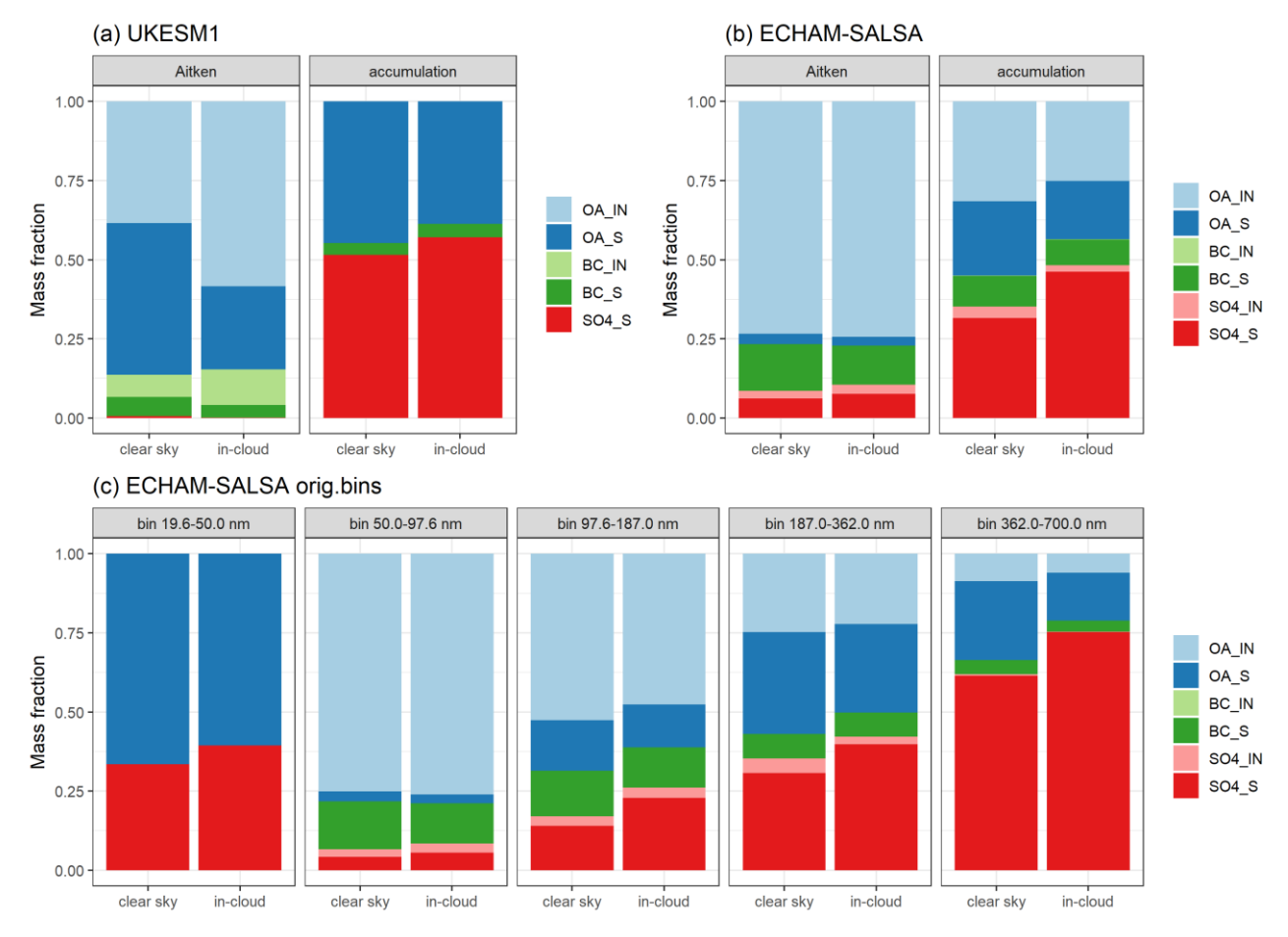


Figure S20 Size resolved chemical composition for clear sky and in-cloud (non-precipitating) air masses for the cold and polluted (CP) sector. UKESM1 is shown in (a) and ECHAM-SALSA in (b) and (c). The notations within the legend in (a)-(b) refer to insoluble (IN) and soluble (S) particle modes, and in (b) the sectional bins from ECHAM-SALSA are assigned into Aitken (bins with diameters ranging from 19.6 nm to 97.6 nm) and accumulation (bins with diameters ranging from 97.6 nm to 700 nm) classes for easier comparison to UKESM1. The original ECHAM-SALSA bins (Table S3) are shown in (c).

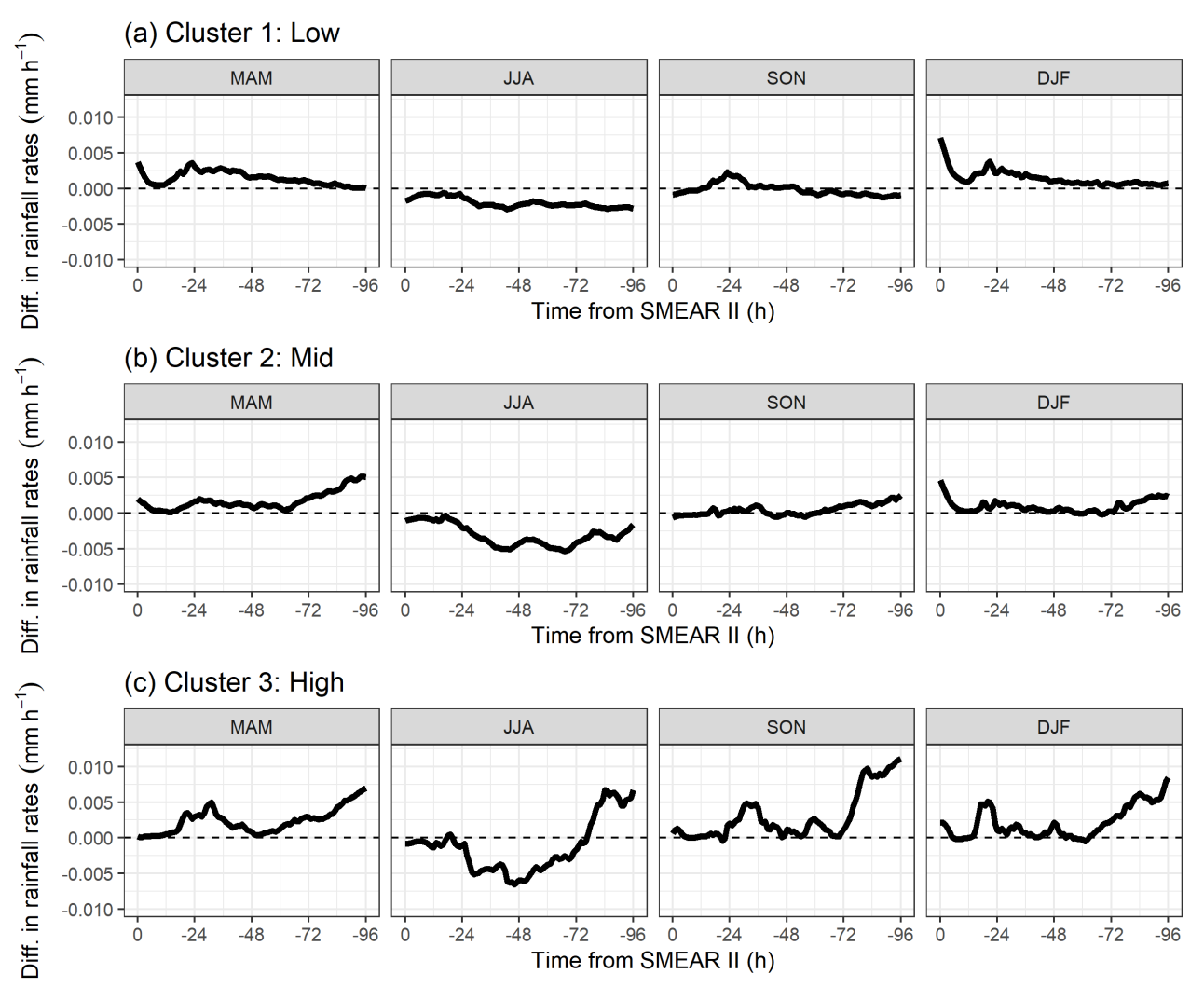


Figure S21 Differences in the mean rainfall rates along the air mass trajectories for each altitude-based cluster with additional seasonal division. The difference is calculated by subtracting the precipitation (liquid, stratiform) at the air mass altitude from the surface precipitation i.e., positive difference indicates the rainfall rates at the surface are higher.

S6 How well RH describes the in-cloud conditions in the GCMs?

To evaluate how well the location of the cloud (1) and non-cloud (0) events at the trajectories agree between the RH (RH > 94 % indicates in-cloud) and cloud fraction (CF > 0.5 indicates in-cloud) based approaches for the two GCMs, we created another cloud proxy from the cloud fraction data. First, we evaluated how well the location of the cloud (1) and non-cloud (0) events at the trajectories agree between the RH and cloud fraction-based approaches. Then, we reproduced the results presented in the main text to see whether the observed effects considering chemical composition of the aerosols stay the same. Overall, same conclusions could be drawn, indicating RH derived cloud proxy is adequate enough for this type of trajectory-based analysis in which the overall effects of clouds are inspected. However, it is important to keep in mind that we are inspecting the average conditions during air mass transport.

To compare how well the location of the cloud (1) and non-cloud events (0) agree between the two approaches, we have used Simple Matching Coefficient (SMC), closely related to the Jaccard coefficient first developed already in late eighteen-hundreds (e.g., Murphy, 1996). It is derived as

$$SMC = \frac{\text{number of matching events}}{\text{number of all events}} = \frac{f_{00} + f_{11}}{f_{10} + f_{01} + f_{00} + f_{11}}.$$
 (S1)

In Eq. (S1) f_{00} and f_{11} are the number of cases when both approaches have non-cloud event (00) or cloud event (11). Similarly, f_{01} and f_{10} refer to cases where the cloud events and non-cloud events are mismatched between the two approaches. Figure S22 shows the SMCs as a time from SMEAR II station for the different sectors inspected. As can be seen from Figure S22, this simple comparison shows the position of in-cloud and non-cloud events is agreeing well with the warm air masses, the cold and clean sector showing largest differences.

Figure S23 shows the mass concentrations of different chemical species for all air mass sectors now using the cloud fraction derived cloud proxy instead when classifying the data into the clear sky and in-cloud groups. Similar to the analysis presented in main text (Section 5), we observe larger SO₄ masses for cloud processed air masses for all other sectors except the warm and clean (Figure S23d).

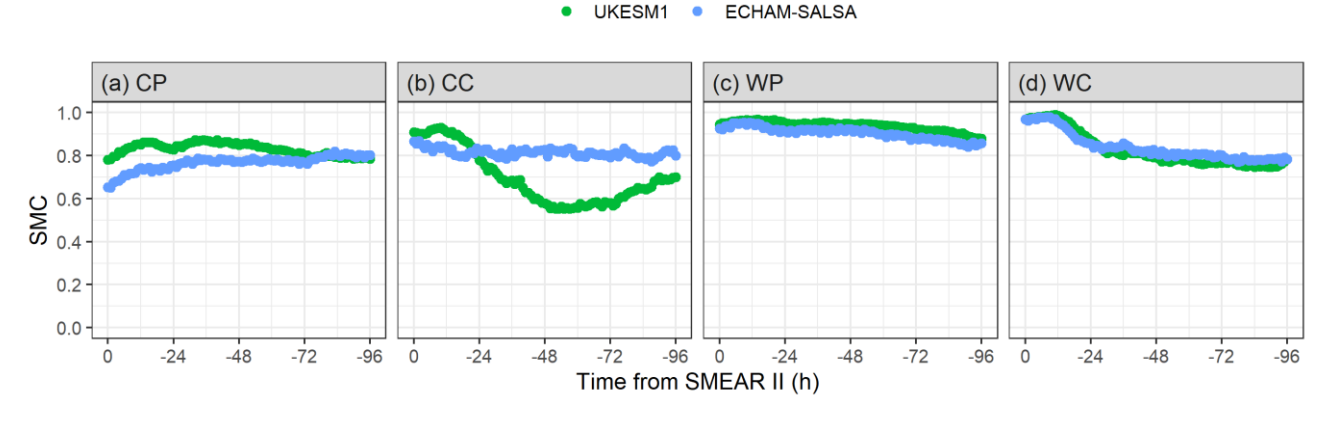


Figure S22 Simple Matching Coefficients (SMC) as a function of time from SMEAR II for different sectors and both GCMs. The data used to calculate the coefficients matches to the chemistry data used in Section 5.

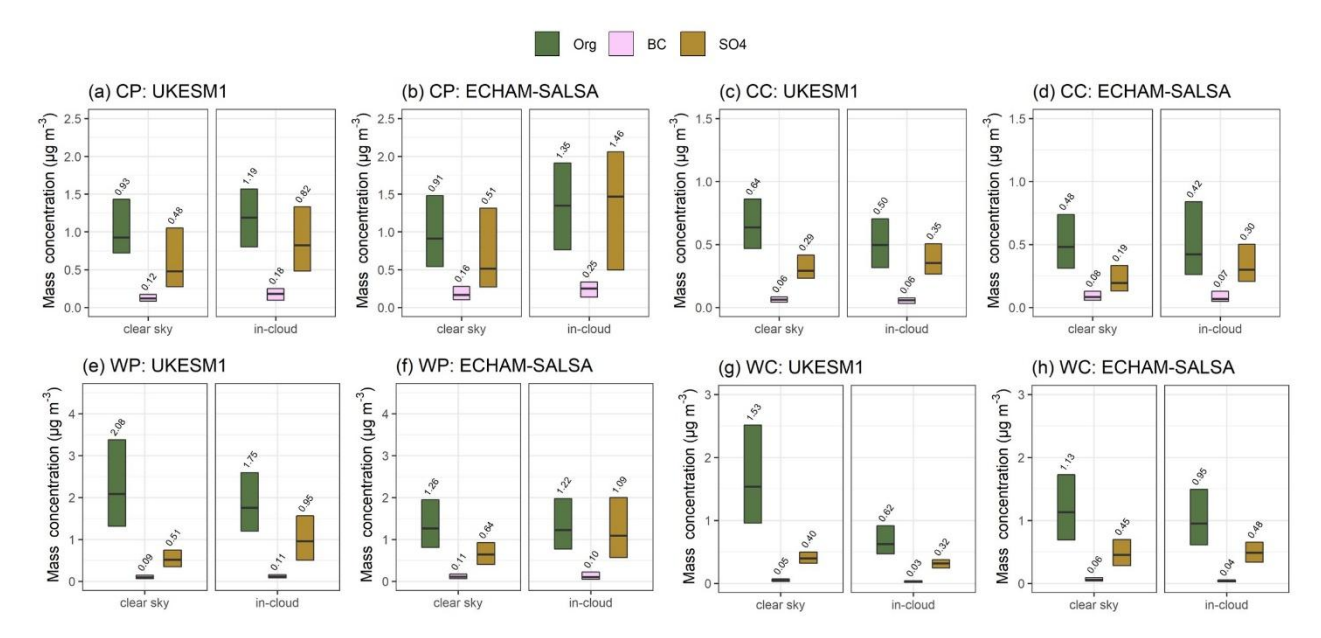


Figure S23 Median (black horizontal lines and numerical values) particle mass concentrations with 25th-75th percentiles (boxes) for OA, BC, and SO4 for all air mass sectors. The experienced conditions by the air mass are denoted as clear-sky and in-cloud (non-precipitating) and the in-cloud conditions are now based on the model cloud fraction data.

Table S10 Statistical significance (p-values) of the differences between the data from clear sky and in-cloud groups (based on cloud fraction derived cloud proxy) for OA, BC and SO4 for each sector for the GCMs (UKESM and SALSA). P-values were obtained by Kruskal-Wallis rank sum test. Values smaller than 0.01 (or 0.05, depending on source literature) indicate the null hypothesis (distributions are identical) could be rejected.

	Sector										
Species	CP: Cold	and polluted	CC: Cold and clean		WP: Warm and polluted		WC: Warm and clean				
	UKESM	SALSA	UKESM	SALSA	UKESM	SALSA	UKESM	SALSA			
OA	< 0.001	< 0.001	< 0.001	0.184	0.013	0.967	< 0.001	0.002			
SO ₄	< 0.001	< 0.001	0.001	< 0.001	< 0.001	< 0.001	< 0.001	0.077			
BC	< 0.001	< 0.001	0.079	0.030	0.026	0.789	< 0.001	< 0.001			

References

Abdul-Razzak, H. and Ghan, S. J.: A parameterization of aerosol activation: 2. Multiple aerosol types, J. Geophys. Res. Atmospheres, 105, 6837–6844, https://doi.org/10.1029/1999JD901161, 2000a.

Abdul-Razzak, H. and Ghan, S. J.: A parameterization of aerosol activation: 2. Multiple aerosol types, J. Geophys. Res. Atmospheres, 105, 6837–6844, https://doi.org/10.1029/1999JD901161, 2000b.

Abdul-Razzak, H. and Ghan, S. J.: A parameterization of aerosol activation 3. Sectional representation, J. Geophys. Res. Atmospheres, 107, AAC 1-1-AAC 1-6, https://doi.org/10.1029/2001JD000483, 2002.

Abraham, N. L., Archibald, A. T., Bellouin, N., Boucher, O., Braesicke, P., Bushell, A., Carslaw, K., Collins, B., Dalvi, M., Dearden, C., Dennison, F., Emmerson, K., Folberth, G., Haywood, J., Hewitt, A., Johnson, C., Kipling, Z., Macintyre, H., Mann, G., Telford, P., Merikanto, J., Morgenstern, O., O'Connor, F., Ordonez, C., Osprey, S., Pringle, K., Pyle, J., Rae, J., Reddington, C., Richardson, M., Savage, N., Sellar, A., Spracklen, D., Stier, P., West, R., Mulcahy, J., Woodward, S., Boutle, I., and Woodhouse, M. T.: Unified Model Documentation Paper 084 - United Kingdom Chemistry and Aerosol (UKCA) Technical Description, UM version 11.1, 2018.

Aerosol GCM Trajectory (GCMTraj) | AeroCom: https://aerocom.met.no/experiments/GCMTraj, last access: 11 October 2024.

Bellouin, N., Rae, J., Jones, A., Johnson, C., Haywood, J., and Boucher, O.: Aerosol forcing in the Climate Model Intercomparison Project (CMIP5) simulations by HadGEM2-ES and the role of ammonium nitrate, J. Geophys. Res. Atmospheres, 116, https://doi.org/10.1029/2011JD016074, 2011.

Bentsen, M., Bethke, I., Debernard, J. B., Iversen, T., Kirkevåg, A., Seland, Ø., Drange, H., Roelandt, C., Seierstad, I. A., Hoose, C., and Kristjánsson, J. E.: The Norwegian Earth System Model, NorESM1-M – Part 1: Description and basic evaluation of the physical climate, Geosci. Model Dev., 6, 687–720, https://doi.org/10.5194/gmd-6-687-2013, 2013.

Croft, B., Lohmann, U., Martin, R. V., Stier, P., Wurzler, S., Feichter, J., Posselt, R., and Ferrachat, S.: Aerosol size-dependent below-cloud scavenging by rain and snow in the ECHAM5-HAM, Atmospheric Chem. Phys., 9, 4653–4675, https://doi.org/10.5194/acp-9-4653-2009, 2009.

Croft, B., Lohmann, U., Martin, R. V., Stier, P., Wurzler, S., Feichter, J., Hoose, C., Heikkilä, U., van Donkelaar, A., and Ferrachat, S.: Influences of in-cloud aerosol scavenging parameterizations on aerosol concentrations and wet deposition in ECHAM5-HAM, Atmospheric Chem. Phys., 10, 1511–1543, https://doi.org/10.5194/acp-10-1511-2010, 2010.

Dietlicher, R., Neubauer, D., and Lohmann, U.: Prognostic parameterization of cloud ice with a single category in the aerosol-climate model ECHAM(v6.3.0)-HAM(v2.3), Geosci. Model Dev., 11, 1557–1576, https://doi.org/10.5194/gmd-11-1557-2018, 2018.

Dietlicher, R., Neubauer, D., and Lohmann, U.: Elucidating ice formation pathways in the aerosol-climate model ECHAM6-HAM2, Atmospheric Chem. Phys., 19, 9061–9080, https://doi.org/10.5194/acp-19-9061-2019, 2019.

Emmons, L. K., Walters, S., Hess, P. G., Lamarque, J.-F., Pfister, G. G., Fillmore, D., Granier, C., Guenther, A., Kinnison, D., Laepple, T., Orlando, J., Tie, X., Tyndall, G., Wiedinmyer, C., Baughcum, S. L., and Kloster, S.: Description and evaluation of the Model for Ozone and Related chemical Tracers, version 4 (MOZART-4), Geosci. Model Dev., 3, 43–67, https://doi.org/10.5194/gmd-3-43-2010, 2010.

Fountoukis, C. and Nenes, A.: Continued development of a cloud droplet formation parameterization for global climate models, J. Geophys. Res. Atmospheres, 110, https://doi.org/10.1029/2004JD005591, 2005.

Ghan, S. J., Leung, L. R., Easter, R. C., and Abdul-Razzak, H.: Prediction of cloud droplet number in a general circulation model, J. Geophys. Res. Atmospheres, 102, 21777–21794, https://doi.org/10.1029/97JD01810, 1997.

Holopainen, E., Kokkola, H., Laakso, A., and Kühn, T.: In-cloud scavenging scheme for sectional aerosol modules – implementation in the framework of the Sectional Aerosol module for Large Scale Applications version 2.0 (SALSA2.0) global aerosol module, Geosci Model Dev, 13, 6215–6235, https://doi.org/10.5194/gmd-13-6215-2020, 2020.

- Hurrell, J. W., Holland, M. M., Gent, P. R., Ghan, S., Kay, J. E., Kushner, P. J., Lamarque, J.-F., Large, W. G., Lawrence, D., Lindsay, K., Lipscomb, W. H., Long, M. C., Mahowald, N., Marsh, D. R., Neale, R. B., Rasch, P., Vavrus, S., Vertenstein, M., Bader, D., Collins, W. D., Hack, J. J., Kiehl, J., and Marshall, S.: The Community Earth System Model: A Framework for Collaborative Research, Bull. Am. Meteorol. Soc., 94, 1339–1360, https://doi.org/10.1175/BAMS-D-12-00121.1, 2013.
- Isokääntä, S., Kim, P., Mikkonen, S., Kühn, T., Kokkola, H., Yli-Juuti, T., Heikkinen, L., Luoma, K., Petäjä, T., Kipling, Z., Partridge, D., and Virtanen, A.: The effect of clouds and precipitation on the aerosol concentrations and composition in a boreal forest environment, Atmospheric Chem. Phys., 22, 11823–11843, https://doi.org/10.5194/acp-22-11823-2022, 2022.
- Kipling, Z., Stier, P., Schwarz, J. P., Perring, A. E., Spackman, J. R., Mann, G. W., Johnson, C. E., and Telford, P. J.: Constraints on aerosol processes in climate models from vertically-resolved aircraft observations of black carbon, Atmos Chem Phys, 13, 5969–5986, https://doi.org/10.5194/acp-13-5969-2013, 2013.
- Kirkevåg, A., Grini, A., Olivié, D., Seland, Ø., Alterskjær, K., Hummel, M., Karset, I. H. H., Lewinschal, A., Liu, X., Makkonen, R., Bethke, I., Griesfeller, J., Schulz, M., and Iversen, T.: A production-tagged aerosol module for Earth system models, OsloAero5.3 extensions and updates for CAM5.3-Oslo, Geosci. Model Dev., 11, 3945–3982, https://doi.org/10.5194/gmd-11-3945-2018, 2018.
- Kokkola, H., Kühn, T., Laakso, A., Bergman, T., Lehtinen, K. E. J., Mielonen, T., Arola, A., Stadtler, S., Korhonen, H., Ferrachat, S., Lohmann, U., Neubauer, D., Tegen, I., Siegenthaler-Le Drian, C., Schultz, M. G., Bey, I., Stier, P., Daskalakis, N., Heald, C. L., and Romakkaniemi, S.: SALSA2.0: The sectional aerosol module of the aerosol–chemistry–climate model ECHAM6.3.0-HAM2.3-MOZ1.0, Geosci Model Dev, 11, 3833–3863, https://doi.org/10.5194/gmd-11-3833-2018, 2018.
- Liu, X., Ma, P.-L., Wang, H., Tilmes, S., Singh, B., Easter, R. C., Ghan, S. J., and Rasch, P. J.: Description and evaluation of a new four-mode version of the Modal Aerosol Module (MAM4) within version 5.3 of the Community Atmosphere Model, Geosci. Model Dev., 9, 505–522, https://doi.org/10.5194/gmd-9-505-2016, 2016.
- Lohmann, U.: Possible aerosol effects on ice clouds via contact nucleation, J. Atmospheric Sci., 59, 647–656, 2002.
- Mann, G. W., Carslaw, K. S., Spracklen, D. V., Ridley, D. A., Manktelow, P. T., Chipperfield, M. P., Pickering, S. J., and Johnson, C. E.: Description and evaluation of GLOMAP-mode: a modal global aerosol microphysics model for the UKCA composition-climate model, Geosci Model Dev, 3, 519–551, https://doi.org/10.5194/gmd-3-519-2010, 2010.
- Marshal, J. S. and Palmer, W. M. K.: The Distribution of Raindrops with Size, J. Meteorol., 5, 165–166, https://doi.org/10.1175/1520-0469(1948)005<0165:TDORWS>2.0.CO;2, 1948.
- Mulcahy, J. P., Jones, C., Sellar, A., Johnson, B., Boutle, I. A., Jones, A., Andrews, T., Rumbold, S. T., Mollard, J., Bellouin, N., Johnson, C. E., Williams, K. D., Grosvenor, D. P., and McCoy, D. T.: Improved Aerosol Processes and Effective Radiative Forcing in HadGEM3 and UKESM1, J. Adv. Model. Earth Syst., 10, 2786–2805, https://doi.org/10.1029/2018MS001464, 2018.
- Mulcahy, J. P., Johnson, C., Jones, C. G., Povey, A. C., Scott, C. E., Sellar, A., Turnock, S. T., Woodhouse, M. T., Abraham, N. L., Andrews, M. B., Bellouin, N., Browse, J., Carslaw, K. S., Dalvi, M., Folberth, G. A., Glover, M., Grosvenor, D. P., Hardacre, C., Hill, R., Johnson, B., Jones, A., Kipling, Z., Mann, G., Mollard, J., O'Connor, F. M., Palmiéri, J., Reddington, C., Rumbold, S. T., Richardson, M., Schutgens, N. A. J., Stier, P., Stringer, M., Tang, Y., Walton, J., Woodward, S., and Yool, A.: Description and evaluation of aerosol in UKESM1 and HadGEM3-GC3.1 CMIP6 historical simulations, Geosci Model Dev, 13, 6383–6423, https://doi.org/10.5194/gmd-13-6383-2020, 2020.
- Murphy, A. H.: The Finley Affair: A Signal Event in the History of Forecast Verification, Weather Forecast., 11, 3–20, https://doi.org/10.1175/1520-0434(1996)011<0003:TFAASE>2.0.CO;2, 1996.
- Neale, R. B., Gettelman, A., Park, S., Chen, C.-C., Lauritzen, P. H., Williamson, D. L., Conley, A. J., Kinnison, D., Marsh, D., Smith, A. K., Vitt, F. M., Garcia, R., Lamarque, J.-F., Mills, M. J., Tilmes, S., Morrison, H., Cameron-Smith, P., Collins, W. D., Iacono, M. J., Easter, R. C., Liu, X., Ghan, S. J., Rasch, P. J., and Taylor, M. A.: Description of the NCAR Community Atmosphere Model (CAM 5.0), https://doi.org/10.5065/wgtk-4g06, 2012.

Neubauer, D., Ferrachat, S., Siegenthaler-Le Drian, C., Stier, P., Partridge, D. G., Tegen, I., Bey, I., Stanelle, T., Kokkola, H., and Lohmann, U.: The global aerosol–climate model ECHAM6.3–HAM2.3 – Part 2: Cloud evaluation, aerosol radiative forcing, and climate sensitivity, Geosci. Model Dev., 12, 3609–3639, https://doi.org/10.5194/gmd-12-3609-2019, 2019.

Slinn, W. G. N.: Precipitation Scavenging, edited by: D., R., U.S. Department of Energy, Washington, D.C., 1983.

Spracklen, D. V., Pringle, K. J., Carslaw, K. S., Chipperfield, M. P., and Mann, G. W.: A global off-line model of size-resolved aerosol microphysics: I. Model development and prediction of aerosol properties, Atmos Chem Phys, 5, 2227–2252, https://doi.org/10.5194/acp-5-2227-2005, 2005.

Stevens, B., Giorgetta, M., Esch, M., Mauritsen, T., Crueger, T., Rast, S., Salzmann, M., Schmidt, H., Bader, J., Block, K., Brokopf, R., Fast, I., Kinne, S., Kornblueh, L., Lohmann, U., Pincus, R., Reichler, T., and Roeckner, E.: Atmospheric component of the MPI-M Earth System Model: ECHAM6, J. Adv. Model. Earth Syst., 5, 146–172, https://doi.org/10.1002/jame.20015, 2013.

Stier, P., Feichter, J., Kinne, S., Kloster, S., Vignati, E., Wilson, J., Ganzeveld, L., Tegen, I., Werner, M., Balkanski, Y., Schulz, M., Boucher, O., Minikin, A., and Petzold, A.: The aerosol-climate model ECHAM5-HAM, Atmos Chem Phys, 5, 1125–1156, https://doi.org/10.5194/acp-5-1125-2005, 2005.

Tegen, I., Neubauer, D., Ferrachat, S., Siegenthaler-Le Drian, C., Bey, I., Schutgens, N., Stier, P., Watson-Parris, D., Stanelle, T., Schmidt, H., Rast, S., Kokkola, H., Schultz, M., Schroeder, S., Daskalakis, N., Barthel, S., Heinold, B., and Lohmann, U.: The global aerosol–climate model ECHAM6.3–HAM2.3 – Part 1: Aerosol evaluation, Geosci Model Dev, 12, 1643–1677, https://doi.org/10.5194/gmd-12-1643-2019, 2019.

Vignati, E., Wilson, J., and Stier, P.: M7: An efficient size-resolved aerosol microphysics module for large-scale aerosol transport models, J. Geophys. Res. Atmospheres, 109, https://doi.org/10.1029/2003JD004485, 2004.

Wang, H., Easter, R. C., Rasch, P. J., Wang, M., Liu, X., Ghan, S. J., Qian, Y., Yoon, J. H., Ma, P. L., and Vinoj, V.: Sensitivity of remote aerosol distributions to representation of cloud–aerosol interactions in a global climate model, Geosci. Model Dev., 6, 765–782, https://doi.org/10.5194/gmd-6-765-2013, 2013.

Wang, Q., Jacob, D. J., Fisher, J. A., Mao, J., Leibensperger, E. M., Carouge, C. C., Le Sager, P., Kondo, Y., Jimenez, J. L., Cubison, M. J., and Doherty, S. J.: Sources of carbonaceous aerosols and deposited black carbon in the Arctic in winter-spring: implications for radiative forcing, Atmos Chem Phys, 11, 12453–12473, https://doi.org/10.5194/acp-11-12453-2011, 2011.

West, R. E. L., Stier, P., Jones, A., Johnson, C. E., Mann, G. W., Bellouin, N., Partridge, D. G., and Kipling, Z.: The importance of vertical velocity variability for estimates of the indirect aerosol effects, Atmospheric Chem. Phys., 14, 6369–6393, https://doi.org/10.5194/acp-14-6369-2014, 2014.

Woodward, S.: Modeling the atmospheric life cycle and radiative impact of mineral dust in the Hadley Centre climate model, J. Geophys. Res. Atmospheres, 106, 18155–18166, https://doi.org/10.1029/2000JD900795, 2001.